Atmos. Chem. Phys. Discuss., 12, 17031–17086, 2012
www.atmos-chem-phys-discuss.net/12/17031/2012/
doi:10.5194/acpd-12-17031-2012

Atmospheric Chemistry and Physics Discussions

Contributions of individual reactive biogenic volatile organic compounds to organic nitrates above a mixed forest

K. A. Pratt[1], L. H. Mielke[1,*], P. B. Shepson[1,2,3], A. M. Bryan[4], A. L. Steiner[4], J. Ortega[5,], R. Daly[5,***], D. Helmig[5], C. S. Vogel[6], S. Griffith[7], S. Dusanter[7,8,9], P. S. Stevens[7,10], and M. Alaghmand[1]**

[1]Department of Chemistry, Purdue University, West Lafayette, IN, USA
[2]Department of Earth and Atmospheric Sciences, Purdue University, West Lafayette, IN, USA
[3]Purdue Climate Change Research Center, Purdue University, West Lafayette, IN, USA
[4]Department of Atmospheric, Oceanic and Space Sciences, University of Michigan, Ann Arbor, MI, USA
[5]Institute of Arctic and Alpine Research, University of Colorado, Boulder, CO, USA
[6]University of Michigan Biological Station, Pellston, MI, USA
[7]School of Public and Environmental Affairs, Indiana University, Bloomington, IN, USA
[8]Université Lille Nord de France, Lille, France
[9]École des Mines de Douai, Douai, France
[10]Department of Chemistry, Indiana University, Bloomington, IN, USA
[*]now at: School of Public and Environmental Affairs, Indiana University, Bloomington, IN, USA

[**] now at: Atmospheric Chemistry Division, Earth System Laboratory, National Center for Atmospheric Research, Boulder, CO, USA
[***] now at: Air Pollution Prevention and Control Division, National Risk Management Research Laboratory, US Environmental Protection Agency, Research Triangle Park, NC, USA

Received: 20 May 2012 – Accepted: 15 June 2012 – Published: 11 July 2012

Correspondence to: K. A. Pratt (kapratt@purdue.edu)

Published by Copernicus Publications on behalf of the European Geosciences Union.

Abstract

Biogenic volatile organic compounds (BVOCs) can react in the atmosphere to form organic nitrates, which serve as NO_x ($NO + NO_2$) reservoirs, impacting ozone and secondary organic aerosol production, the oxidative capacity of the atmosphere, and nitrogen availability to ecosystems. To examine the contributions of biogenic emissions and the formation and fate of organic nitrates in a forest environment, we simulated the oxidation of 57 individual BVOCs emitted from a rural mixed forest in Northern Michigan. Of the total simulated organic nitrates, monoterpenes contributed ∼70 % in the early morning at ∼12 m above the forest canopy when isoprene emissions were low. In the afternoon, when vertical mixing and isoprene nitrate production were highest, the simulated contribution of isoprene-derived organic nitrates was greater than 90 % at all altitudes, with the concentration of secondary isoprene nitrates increasing with altitude. Key BVOC-oxidant reactions were identified for future laboratory and field investigations into reaction rate constants, yields, and speciation of oxidation products. Forest succession, wherein aspen trees are being replaced by pine and maple trees, was predicted to lead to increased afternoon concentrations of monoterpene-derived organic nitrates. This further underscores the need to understand the formation and fate of these species, which have different chemical pathways and oxidation products compared to isoprene-derived organic nitrates and can lead to secondary organic aerosol formation.

1 Introduction

Globally, biogenic volatile organic compound (BVOC) emissions (∼1150 $\mathrm{Tg\,C\,yr^{-1}}$) comprise ∼90 % of total non-methane VOC emissions, and isoprene and monoterpenes alone are estimated to account for ∼48 % of total non-methane VOC emissions (Guenther et al., 1995; Goldstein and Galbally, 2007). These BVOCs typically have atmospheric lifetimes of minutes to hours for reactions with the hydroxyl (OH) radical, ozone (O_3), and the nitrate (NO_3) radical (Atkinson and Arey, 2003b). In the atmosphere, BVOCs exist as complex mixtures with individual BVOC mole fractions ranging from a few ppb to sub-ppt (Bouvier-Brown et al., 2009). The chemistry and fate of atmospheric BVOCs have important implications for ozone and secondary organic aerosol production, yet many questions remain regarding these processes (Goldstein and Galbally, 2007).

Tropospheric ozone is produced via oxidation of NO to NO_2 by organic peroxy radicals and HO_2 (e.g. Hauglustaine et al., 1996). Organic nitrates serve as NO_x ($NO + NO_2$) reservoirs. Therefore, they impact nitrogen availability to ecosystems (Lockwood et al., 2008), ozone production (both locally and downwind) (e.g. Fiore et al., 2005; Wu et al., 2007), and the oxidative capacity of the atmosphere, impacting trace gas removal and secondary organic aerosol formation and processing (e.g. Rollins et al., 2010). Organic nitrates ($RONO_2$) are formed via reactions of VOCs with OH in the presence of NO, as shown in reactions 1–3, which show H-atom abstraction from a C–H bond, followed by O_2 addition yielding a peroxy radical that can react with NO to produce $RONO_2$ (Orlando et al., 2003).

$$RH + {}^{\cdot}OH \rightarrow R^{\cdot} + H_2O \tag{R1}$$

$$R^{\cdot} + O_2 \rightarrow RO_2^{\cdot} \tag{R2}$$

$$RO_2^{\cdot} + NO \rightarrow RONO_2 \tag{R3}$$

Alternatively, organic nitrates can also be formed from VOCs through addition of NO_3 or OH, followed by peroxy radical formation and reaction with NO. Olefins constitute the largest VOC emission flux globally, and OH reactions with olefins are primarily via addition. Therefore, most organic nitrates are “multifunctional” (O’Brien et al., 1995) and not simple “alkyl nitrates”, produced via H-atom abstraction. Organic nitrates have been shown to be a major component (12–20 %) of NO_y (measured as $NO + NO_2 + HNO_3$ + peroxy acetyl nitrates + $RONO_2$) over the Eastern US during summer (Perring et al., 2009a). During the aircraft-based study by Perring et al. (2009a),

~75 % of the organic nitrates below 0.5 km were estimated to be derived from isoprene. At night, isoprene nitrates formed via reaction of isoprene with NO_3 were estimated to comprise 2–9 % of NO_y (Brown et al., 2009). Correspondingly, modeled tropospheric ozone production rates and concentrations are sensitive to isoprene emission rates and the yield of isoprene nitrates (Fiore et al., 2005; Wu et al., 2007). Further, the fate of organic nitrates and associated recycling of NO_x is highly uncertain, even for isoprene, the most abundant BVOC (Horowitz et al., 2007).

While the measurement of a large contribution of organic nitrates to NO_y raises important questions about their nature and sources, measurement of the contributions of specific $RONO_2$ compounds in the atmosphere remains an analytical challenge, due to low ambient concentrations and the adsorptive nature of multifunctional nitrates (e.g. Muthuramu et al., 1993). Thus, few atmospheric measurements of speciated organic nitrates from BVOC precursors exist; in fact, only select nitrates resulting from isoprene oxidation have been measured (Werner et al., 1999; Grossenbacher et al., 2001, 2004; Giacopelli et al., 2005; Beaver et al., 2012). Isolation of specific $RONO_2$ isomers is further complicated by secondary chemistry and loss processes (Giacopelli et al., 2005), the contributions of which change spatially and temporally (Day et al., 2003).

The rural mixed forest environment at the University of Michigan Biological Station (UMBS) in Northern Michigan is an excellent location for studying the atmospheric chemistry of a wide variety of individual BVOCs. At this site, the forest composition and succession are well characterized (Bergen and Dronova, 2007), and the tree species-specific fluxes of BVOCs have been measured (Ortega et al., 2007, 2008). Together, this unique information and the well-studied atmospheric environment at UMBS represent a unique opportunity to study the specifics of BVOC-derived organic nitrate production. This study utilized a simple atmospheric chemistry one-dimensional model to simulate the formation and fate of organic nitrates produced from the oxidation of 57 individual BVOCs locally emitted at UMBS. Several previous studies of BVOCs have utilized more complex one-dimensional modeling to gain insight into local-scale chemistry (Trainer et al., 1991; Gao et al., 1993; Makar et al., 1999; Spanke et al., 2001; Stroud et al., 2005; Forkel et al., 2006; Boy et al., 2011; Mogensen et al., 2011; Wolfe and Thornton, 2011; Wolfe et al., 2011a, b). These recent BVOC-focused modeling studies combine detailed micrometeorology with atmospheric chemistry to simulate chemistry in and above the forest canopy. The goal of this study was to investigate the full suite of the 57 BVOCs observed to be emitted in the UMBS forest; however, existing chemical mechanisms cannot capture this large number of BVOC species. For example, one of the most complex mechanisms at this time is the Master Chemical Mechanism (MCM, http://mcm.leeds.ac.uk/MCM); yet of the BVOCs emitted at UMBS, this mechanism only includes isoprene, α-pinene, β-pinene, limonene, and β-caryophyllene. Further, most chemical mechanisms require lumped species, not allowing the examination of individual BVOCs. These various BVOCs are characterized by different and complex chemical structures, resulting in variations in reactivity, as well as different oxidation products with subsequently different lifetimes. Therefore, the model herein includes a simplified atmospheric treatment with more complex chemistry to investigate the contributions of the full suite of observed BVOCs to organic nitrate production and concentrations with respect to time of day and height above the forest canopy. As the aspen forests (*Populus grandidentata* and *Populus tremuloides*) in the upper Great Lakes region are maturing and will be replaced by northern hardwoods (*Acer rubrum*, *Acer saccharum*, *Fagus grandifola*) and upland pine (*Pinus strobus*, *Pinus resinosa*) (Bergen and Dronova, 2007), the impacts of forest succession on atmospheric composition are also examined. The focus of this study was to highlight the role of individual BVOC contributions to organic nitrate formation and to identify key species that require further examination in future laboratory and field studies.

2 Experimental

2.1 Measurements

Atmospheric summertime BVOC emissions and oxidation chemistry were evaluated in Northern Michigan at the Program for Research on Oxidants: Photochemistry, Emissions and Transport (PROPHET) tower site at the University of Michigan Biological Station (UMBS, 45° 30′ N, 84° 42′ W, elevation 238 m) in Northern Michigan (Carroll et al., 2001). An AmeriFlux site is located 132 m north-northeast of the PROPHET tower. The nearest town is Pellston, Michigan (population <800), located ~5.5 km to the west; Detroit, Michigan is the nearest major metropolitan area, ~350 km to the southeast. To eliminate the need to account for wet deposition, only sunny and partly sunny days with no precipitation in July–August 2008 were considered for the following analysis. Ambient air measurements of isoprene, total monoterpenes, methacrolein (MACR), and methyl vinyl ketone (MVK) were conducted using the proton-transfer reaction linear ion trap mass spectrometer (PTR-LIT), described previously by Mielke et al. (2008, 2010), at ~34 m above ground (~12 m above canopy) at UMBS in July–August 2008. NO, NO_2, total $RONO_2$, and NO_y^* ($\sim NO_y$-HNO_3) were measured using a custom chemiluminescence instrument with thermal decomposition inlets, constructed following the designs of Ridley and Grahek (1990), Bollinger et al. (1983), and Day et al. (2002). All times are given in Eastern Standard Time (EST), one hour behind Eastern Daylight Time.

2.2 Model description

A simplified atmospheric chemistry one-dimensional model was constructed to simulate the emissions, transport, and reactions of 57 locally-produced BVOCs at the UMBS PROPHET site. The atmosphere was represented by 25 vertical bins, including 2 bins within the forest canopy, extending from 12 m above the surface to approximately 4 km; due to the simplicity of the canopy bins, atmospheric chemistry is only discussed for the bins above the forest canopy. BVOC concentrations were calculated according to transport and reaction kinetics following Eq. (1), which describes the change in the concentration of VOC i at altitude z and time t ($c_i(z,t)$):

$$\frac{\mathrm{d}c_i(z,t)}{\mathrm{d}t} = E_i(z,t) + P_i(z,t) + \frac{F_{\downarrow,i}(z,t)}{h_z} - L_i(z,t) - \frac{F_{\uparrow,i}(z,t)}{h_z} - \frac{D_i(z,t)}{h_z} - H_i(z,t) \tag{1}$$

VOC terms, described below, include emission (E) into the first canopy bin, chemical production (P) and loss (L) based on chemical kinetics, upward and downward vertical fluxes ($F_\uparrow$ and $F_\downarrow$, respectively) divided by bin height (h), dry deposition (D), and horizontal advection (H).

2.2.1 BVOC emissions

Based on mean green-leaf dry mass, characterized during litter trap studies of 101 plots in 2008 and 2010, the local UMBS forest (1.4 km^2) is primarily composed of bigtooth aspen (*Populus grandidenta*, ∼23 %), red maple (*Acer rubrum*, ∼23 %), red oak (*Quercus rubra*, ∼22 %), quaking aspen (*Populus tremuloides*, ∼8 %), sugar maple (*Acer saccharum*, ∼7 %), paper birch (*Betula papyrifera*, ∼7 %), white pine (*Pinus strobus*, ∼7 %), American beech (*Fagus grandifolia*, ∼3 %), and red pine (*Pinus resinosa*, ∼1 %). The average canopy height is ∼22 m. Speciated emission rates were measured from these individual tree species by branch-enclosure experiments, including measurements at UMBS during the summers of 2003, 2005 (Ortega et al., 2007, 2008), 2009 and 2010; thus, these emission rate measurements are expected to be characteristic of the modeled summer emissions. A total of 57 BVOCs were identified, including isoprene, 2 aromatics, 3 alkanes, 20 monoterpenes (MTs), 8 oxygenated species, and 23 sesquiterpenes (SQTs), and are shown in Table 1. To estimate emission rates for the whole canopy, the basal emission rates (µg C g^{-1} h^{-1}) for each compound were multiplied by the mean green-leaf dry mass (g m^{-2}) for each tree species, obtained through litter trap studies. To estimate future BVOC emissions due to forest succession predicted by Bergen and Dronova (2007), a simplified replacement of aspen (*Populus grandidentata, Populus tremuloides*) by northern hardwoods (*Acer rubrum, Acer saccharum, Fagus grandifola*) or upland pine (*Pinus strobus, Pinus resinosa*) was carried out and is described in the supporting information.

Since isoprene emission is both temperature- and light-dependent, its diurnal emission rates were calculated according to the algorithm given by Guenther et al. (1993), which includes light and temperature correction factors (C_{PAR} and C_T, respectively):

$$\text{ER}(T,\text{PAR}) = \text{ER}(T_\text{s}) \cdot C_{\text{PAR}} \cdot C_T \tag{2}$$

$\text{ER}(T_\text{s})$ is the normalized basal isoprene emission rate at a standard temperature of 303.15 K and a standard photosynthetic active radiation (PAR) flux of 1000 µmol m^{-2} s^{-1}. The light correction factor C_{PAR} is given by:

$$C_{\text{PAR}} = \frac{\alpha c_{L1}\text{PAR}}{\sqrt{1+\alpha^2\text{PAR}^2}} \tag{3}$$

α (= 0.0021) and c_{L1} (= 1.013) are coefficients to account for shading that were calculated according to Guenther et al. (1999) (Eqs. 4b, c) using a measured leaf area index of 3.1 m^2 m^{-2} and assuming equal distribution across the 8.8 m primary canopy bin; these calculated values are similar to those measured by Guenther et al. (1993). Photosynthetic photon flux density was measured at 46 m above ground at the AmeriFlux tower using a LI-COR PAR sensor. The temperature correction factor C_T is given by:

$$C_T = \frac{\exp\dfrac{c_{T1}(T-T_\text{s})}{\text{R}T_\text{s}T}}{1+\exp\dfrac{c_{T2}(T-T_M)}{RT_\text{s}T}} \tag{4}$$

where T is the temperature measured at the PROPHET tower at 32 m, R is the ideal gas constant (8.314 J K^{-1} mol^{-1}), T_s is the standard temperature (303.15 K), and c_{T1}

($950\,000\,\mathrm{J\,mol^{-1}}$), c_{T2} ($230000\,\mathrm{J\,mol^{-1}}$), and T_M (314 K) are empirical coefficients given by Guenther et al. (1993).

At UMBS, MT and SQT emissions are primarily driven by temperature. This was parameterized by an empirical β-factor, measured for the different tree species during branch-enclosure experiments. Therefore, the diurnal emission rates of the BVOCs were calculated according to Guenther et al. (1993):

$$\mathrm{ER}(T) = \mathrm{ER}(T_\mathrm{s}) \cdot \exp\beta(T - T_\mathrm{s}) \tag{5}$$

$\mathrm{ER}(T_\mathrm{s})$ is the BVOC emission rate at a standard temperature of 303.15 K. Previous measurements of MT β-factors showed an average value of $0.14\,\mathrm{K^{-1}}$ with inner-quartile ranges of 0.11–$0.17\,\mathrm{K^{-1}}$; the corresponding average SQT β-factor was $0.17\,\mathrm{K^{-1}}$ with an inner-quartile range of 0.15–$0.21\,\mathrm{K^{-1}}$ (Ortega et al., 2008). These average, upper, and lower β-factors were utilized for the base, minimum, and maximum production rate scenarios, described below. Of the monoterpenes considered here, *trans*-ocimene has been shown to be light- and temperature-dependent (Ortega et al., 2007). Thus, the *trans*-ocimene emission rates were scaled by the light correction factor C_PAR (Eq. 3) and an exponential temperature dependence (Eq. 5).

BVOC emissions were found to vary considerably between individual trees at UMBS (Ortega et al., 2008), similar to previous observations elsewhere by Guenther et al. (1991). Therefore, to examine the model sensitivity to BVOC emissions, three emissions scenarios were constructed as described in the supporting information. For this study, the base production scenario values are reported, with minimum and maximum values reported in brackets, to evaluate the impacts of measurement uncertainties and emission variability. BVOC volumetric production rates (molecules $\mathrm{m^{-3}\,s^{-1}}$) were calculated by dividing the BVOC fluxes (molecules $\mathrm{m^{-2}\,s^{-1}}$) by the height of the first canopy bin (8.8 m), which extends from 12.1–20.9 m above the ground and covers the majority of the leaf biomass at the site (Schmid et al., 2003). As noted above, for the light-dependent BVOCs isoprene and *trans*-ocimene, shading within the large canopy bin is accounted for using the coefficients α and c_{L1}. Despite the fact that multiple finely-resolved canopy bins are not utilized in this model, there is good agreement between measured and modeled above-canopy VOC concentrations (discussed below). This suggests that our treatment with BVOCs being emitted into one large canopy bin is sufficient for the purposes of understanding the local contributions of individual BVOCs to biogenic organic nitrate formation.

2.2.2 Vertical transport

The vertical flux of each chemical species, denoted as $F_{\uparrow}$ and $F_{\downarrow}$ for positive and negative vertical fluxes, respectively, was calculated as:

$$F_{\uparrow,i} = -K_{H,z}\frac{\Delta[\mathrm{VOC}_i]}{\Delta z} \tag{6}$$

where $\Delta[\mathrm{VOC}_i]$ is the concentration difference between neighboring altitude bins, and Δz is the vertical distance between the centers of these two bins. The vertical transport of BVOCs following emission was described by thermal eddy diffusivity (K_H) profiles based on modeled mixing by the CACHE model (Forkel et al., 2006; Bryan et al., 2012) for sunny and partly sunny days during the summer 2009 CABINEX campaign at UMBS. Mixing within the canopy and up to 1.5 times the canopy height (1.5*h*) was parameterized with a modified *K*-theory that uses observations of vertical velocity standard deviation at two heights within and above the canopy (0.92*h* and 1.5*h*) to account for "near-field" mixing effects (Raupach, 1989). Modeled K_H values were linearly interpolated from the modeled K_H at the base of the crown space (6 m) to the first (20.6 m; 0.92*h*) and second (34 m; 1.5*h*) measurement heights. In this region, K_H was scaled by the R factor (Eq. 10 in Makar et al., 1999) using a τ/T_L ratio of 4 (Stroud et al., 2005; Wolfe and Thornton, 2011), where τ is the transport lifetime and T_L is the Lagrangian timescale. Above the canopy, modeled values according to Forkel et al. (1990) were used up to approximately 4 km above ground and adjusted to remove the sharp discontinuity between the measurement height and the adjacent model level. The vertical

K_H profile peaks at ~287 m above ground (14:45 EST) with a maximum mixing height of 1 km (Fig. S1, see Supplement), following Gao et al. (1993).

2.2.3 BVOC reactions and oxidant measurements

Once emitted into the model atmosphere, individual BVOCs reacted with OH, O_3, and NO_3. Rather than explicitly calculating oxidant concentrations, 0.5-h resolution average diurnal profiles of OH, O_3, and NO_3 were directly input to minimize uncertainties in O_3 production (Wu et al., 2007) and OH recycling under low NO_x conditions (e.g. Sillman et al., 2002; Hofzumahaus et al., 2009). Above-canopy (32 m above ground) daytime (8:30–18:30) and nighttime [OH] were measured by laser-induced fluorescence (Dusanter et al., 2009) in July–August 2008 and July–August 2009, respectively; these data were combined to provide a full diurnal OH profile. Ozone was measured at 32 m above ground using a Thermo Environmental Instruments model 49C UV absorption ozone analyzer. The 0.5 hr resolution average diurnal profile of NO_3 radical concentrations was calculated using the model described by Hurst et al. (2001); details and modifications are provided in the supporting information. Oxidant concentrations were assumed to be constant with altitude since no vertically-resolved measurements have been made at UMBS. However, previous modeling scenarios for other locations suggest that [O_3] and [NO_3] may increase slightly with increasing height above the forest canopy, while [OH] may increase with height above the canopy in the daytime and decrease above the canopy at night (Gao et al., 1993; Geyer and Stutz, 2004b, 2004a). However, as discussed below, much of the BVOC oxidation occurs in the lowest ~100 m of the boundary layer.

The chemical reaction loss of each VOC at each time step within each bin was calculated as:

$$L_i = k_{\mathrm{OH},i} \cdot [\mathrm{OH}] \cdot [\mathrm{VOC}_i] \cdot \Delta t + k_{\mathrm{O_3},i} \cdot \left[\mathrm{O_3}\right] \cdot [\mathrm{VOC}_i] \cdot \Delta t + k_{\mathrm{NO_3},i} \cdot \left[\mathrm{NO_3}\right] \cdot [\mathrm{VOC}_i] \cdot \Delta t \qquad (7)$$

where t is the model time step (0.2 s) and $k_{\mathrm{OH},i}$, $k_{\mathrm{O_3},i}$, and $k_{\mathrm{NO_3},i}$ are the respective OH, O_3, and NO_3 rate constants for VOC_i, as shown in Table 1. When rate constants were not available, they were calculated using the US Environmental Protection Agency Estimation Program Interface Suite (USEPA, 2010) and the structure activity relations described by Pfrang et al. (2006) and Kerdouci et al. (2010).

Given the abundance of isoprene at UMBS, concentrations of major first-generation isoprene oxidation products MACR and MVK were calculated based on reacted isoprene concentrations and measured yields (Ruppert and Becker, 2000) (Table S3). The isoprene first-generation C_5-unsaturated hydroxyaldehyde isomers, referred to as IP-HMY and IP-MHY, were calculated based on Carter and Atkinson (1996) and Costa (2011) (see Table S3).

2.2.4 Organic nitrates

Few laboratory studies have measured organic nitrate ($RONO_2$) yields from BVOC oxidation. In fact, of the 57 BVOCs considered here, $RONO_2$ yields have only been measured for isoprene (Tuazon and Atkinson, 1990; Chen et al., 1998; Chuong and Stevens, 2002; Sprengnether et al., 2002; Patchen et al., 2007; Perring et al., 2009b; Rollins et al., 2009; Lockwood et al., 2010; Costa, 2011), α-pinene (Hallquist et al., 1999; Nozière et al., 1999; Spittler et al., 2006), β-pinene (Hallquist et al., 1999; Davis et al., 2005; Fry et al., 2009), and limonene (Hallquist et al., 1999; Leungsakul et al., 2005; Spittler et al., 2006; Fry et al., 2011). Therefore, for the remaining BVOCs and primary organic nitrate species, organic nitrate yields for reaction of BVOCs with OH, and subsequently NO, were first estimated based on the number of carbon atoms within each BVOC:

$$\gamma = (0.0381 \pm 0.0031)\,n - (0.073 \pm 0.0178) \qquad (8)$$

where n is equal to the number of carbon atoms (Arey et al., 2001). To apply this parameterization to alkenes, the calculated yield was multiplied by 0.58, according to O'Brien et al. (1998). For compounds with oxygen-containing functional groups present in positions β or further from the peroxy radical, the calculated yield was multiplied by

1.7 (Espada and Shepson, 2005). The production of organic nitrate i was calculated as:

$$P_{\mathrm{ON},i} = k_{\mathrm{OH},i} \cdot [\mathrm{OH}] \cdot [\mathrm{VOC}_i] \cdot \Delta t \cdot \gamma_{\mathrm{OH},i} \cdot \beta + k_{\mathrm{NO_3},i} \cdot \left[\mathrm{NO_3}\right] \cdot [\mathrm{VOC}_i] \cdot \Delta t \cdot \gamma_{\mathrm{NO_3},i} \qquad (9)$$

where γ is the $RONO_2$ yield from the reaction of VOC_i with either OH or NO_3. Since NO was not explicitly calculated within the model, low NO_x conditions were accounted for by the term β, which describes the fraction of time RO_2 reacts with NO versus HO_2 and RO_2, as previously described by Barket et al. (2004):

$$\beta = \frac{k_{\mathrm{RO_2,NO}}[\mathrm{RO_2}][\mathrm{NO}]}{k_{\mathrm{RO_2,NO}}[\mathrm{RO_2}][\mathrm{NO}] + k_{\mathrm{RO_2,HO_2}}[\mathrm{RO_2}][\mathrm{HO_2}] + k_{\mathrm{RO_2,RO_2}}[\mathrm{RO_2}][\mathrm{RO_2}]} \qquad (10)$$

where NO was measured using a customized chemiluminescence instrument, described above, HO_2 was measured using laser-induced fluorescence (Dusanter et al., 2009), and $[RO_2]$ was assumed to equal $[HO_2]$ (Tan et al., 2001; Mihele and Hastie, 2003). The associated rate constants, based on isoprene reactions, are 9.0×10^{-12}, 3.9×10^{-12}, and 1.3×10^{-11} $\mathrm{cm^3\,molec^{-1}\,s^{-1}}$ for $k_{\mathrm{RO_2,NO}}$, $k_{\mathrm{RO_2,HO_2}}$, and $k_{\mathrm{RO_2,RO_2}}$, respectively (Barket et al., 2004). It should be noted that recent studies have found that instruments that detect HO_2 radicals using chemical conversion to OH by reaction with added NO may be sensitive to the detection of hydroxyalkyl peroxy radicals produced from the OH-initiated oxidation of alkenes (Fuchs et al., 2011). As a result, the HO_2 measurements in this study likely represent an upper limit to the actual concentration of HO_2 radicals; thus, the calculated β and corresponding nitrate production represent lower limits.

Speciated primary and secondary isoprene nitrates were estimated based on the laboratory studies of Lockwood et al. (2010), Rollins et al. (2009), Paulot et al. (2009), and Costa (2011) (Table S4). Structures of all other primary and secondary BVOC nitrates produced by reactions with each oxidant (OH, O_3, and NO_3) were estimated (based on known chemistry for proxy compounds) to allow estimation of the corresponding rate constants using the US EPA Estimation Program Interface Suite (USEPA, 2010), as well the structure activity relations described by Pfrang et al. (2006) and Kerdouci et al. (2010). Retention of the nitrate group upon reaction of the primary organic nitrates with OH, O_3, or NO_3 was defined to occur 98 % of the time for all BVOCs except isoprene, which was explicitly described, α-phellandrene (defined as 49 % based on structure estimation for reaction with OH or O_3), and β-phellandrene (defined as 0 %, complete loss, based on structure estimation for reaction with OH or O_3). Secondary dinitrates were predicted to form based on organic nitrate yields, described above, for all BVOCs except α-phellandrene (0.5 dinitrate yield assumed) and β-phellandrene (no dinitrate formation assumed). Nitrate structures were estimated based on trends in bond reactivity and previous studies of organic nitrate formation (Shepson, 2007). A goal of this study was to highlight potentially important BVOC-oxidant chemistry that should be studied further; therefore, the absolute concentrations of organic nitrates reflect the simulation assumptions and should be evaluated by further laboratory studies.

2.2.5 Advection and dry deposition

To examine the impact of only local BVOC emissions and chemistry, the forest canopy was assumed to be the only source of BVOCs. BVOCs and reaction products were removed via horizontal advection (H_i) from the above canopy bins based on horizontal loss rate constants (k_{wind}) defined as:

$$k_{\text{wind}} = \frac{U(z)}{30\,\text{km}} \tag{11}$$

$U(z)$ is the wind speed at a given altitude (in $\text{km}\,\text{s}^{-1}$). While there is heterogeneity in the forest canopy within and near UMBS (Bergen and Dronova, 2007), a homogeneous forest path length of 30 km is assumed, based on the approximate distance from UMBS to Lakes Huron and Michigan. Measurements of wind speeds at 46 m at the AmeriFlux tower using a Campbell Scientific CSAT3 sonic anemometer were used to derive friction velocities (u_*); using Eq. (12), vertically-resolved wind speeds were calculated and are shown in Fig. S2.

$$U(z) = \frac{u_*}{\mathrm{k}} \ln\left(\frac{z-d}{z_0}\right) \tag{12}$$

d is the zero-plane displacement, defined as 0.75 × canopy height (22.0 m), k is the von Karman constant (0.40), z is the bin height, and z_0 is the aerodynamic surface roughness length (2.0 m), calculated based on the Monin-Obukhov length during neutral atmospheric stability conditions.

Reaction products were removed via dry deposition from the two canopy bins (starting at 12.1 m and 20.9 m above ground, respectively). Dry deposition loss (D_i) was defined by the species specific deposition velocity (v_d):

$$D_i = v_{\mathrm{d},i} \cdot [\mathrm{VOC}_i] \cdot \Delta t \tag{13}$$

Dry deposition velocities of organic nitrates are thought to range between that of peroxyacetyl nitrate (PAN, 0.5 $\mathrm{cm\,s^{-1}}$) and $\mathrm{HNO_3}$ (4–5 $\mathrm{cm\,s^{-1}}$) (Grossenbacher et al., 2001). For a pine forest, Farmer and Cohen (2008) calculated a summer mid-day deposition velocity of 2.7 $\mathrm{cm\,s^{-1}}$ for total $\mathrm{RONO_2}$. Daytime dry deposition velocities (v_d) were assumed as follows: first-generation isoprene oxidation products (0.5 $\mathrm{cm\,s^{-1}}$) (Zhang et al., 2003), primary organic nitrates (1.5 $\mathrm{cm\,s^{-1}}$), and secondary organic nitrates (2.5 $\mathrm{cm\,s^{-1}}$). Nighttime dry deposition velocities were assumed to be 10 % of daytime values, following Ganzeveld et al. (2008).

3 Results and discussion

3.1 BVOC emissions and concentrations

The predicted isoprene emission rate diurnal cycle (Fig. S3, mid-day average canopy top flux of 3.5 [1.1–6.2] $\mathrm{mg\,C\,m^{-2}\,h^{-1}}$) agrees well with previous eddy covariance measurements at UMBS with average mid-day fluxes of 2.8, 3.2, and 2.9 $\mathrm{mg\,C\,m^{-2}\,h^{-1}}$

for the summers of 2000–2002 (Pressley et al., 2005). For the base production scenario, simulated isoprene emissions (2.9×10^{19} molecules $\mathrm{m}^{-2}\,\mathrm{h}^{-1}$) comprised 95 % of all BVOCs emitted on a molar basis from the UMBS forest at the time of maximum total BVOC emissions (14:00 EST) (Fig. S3). As shown in Fig. 1, the modeled isoprene vertical profile at 17:00 EST is in agreement with previous measurements made at UMBS at the same time of day (Hurst et al., 2001). In the daytime, the isoprene concentrations at ~12 m above the forest canopy agree with measured values (Fig. 2), similar to previous modeling by Sillman et al. (2002). However, at night (22:00–06:00 EST) modeled isoprene concentrations were lower than observed, with increasing biases through the night. Previous studies using a 0-D model found that the observed isoprene decay rate in the late evening at UMBS was over-predicted, and they hypothesized that this was due to uncertainties in vertical mixing estimates and/or an unknown dark isoprene emission source (Hurst et al., 2001). Uncertainties associated with calculated NO_3 radical concentrations cannot account for the isoprene concentrations (Hurst et al., 2001). Here we included a simple estimate of vertical mixing and found that isoprene concentrations were still under-predicted at night. This further suggests the presence of a nighttime isoprene emission source, estimated previously by Faloona et al. (2001) to be ~2–30 $\mu\mathrm{g}\,\mathrm{m}^{-2}\,\mathrm{h}^{-1}$ in the summer at UMBS.

The discrepancy between measured and modeled isoprene concentrations at night is unlikely to be caused by overestimating [OH] because modeled concentrations of methyl vinyl ketone (MVK) and methacrolein (MACR) are also underpredicted at night (00:00–08:00 EST) (Fig. 2). Additionally, the modeled ratios of [MVK + MACR]/[Isoprene] and [MVK]/[MACR] agree with measurements (Fig. S4). The observed small underprediction of daytime MVK and MACR concentrations is expected because we included only the oxidation of locally emitted BVOCs and did not advect BVOC oxidation products to the site. Overall, the measured and modeled BVOC concentrations were within the ranges of daytime variability. A detailed study of isoprene emission and oxidation in the nocturnal boundary layer should be completed to further our understanding of these processes, including the contributions from upwind advection.

At night, simulated MT and SQT emissions (~3–4 × 10^{17} molecules m^{-2} h^{-1} and ~2–4 × 10^{16} molecules m^{-2} h^{-1}, respectively) comprised ~79–82 % and ~7 %, respectively, of total BVOC emissions; the remaining minor fraction of emissions were due to other BVOCs, including oxygenated species, shown in Table 1. Modeled mid-day canopy-scale emission rates of total MTs and SQTs (0.23 [0.04–0.61] mg m^{-2} h^{-1} and 0.03 [0.001–0.09] mg m^{-2} h^{-1}, respectively) were close to previous estimates (0.21 ± 0.06 mg m^{-2} h^{-1} and 0.10 ± 0.05 mg m^{-2} h^{-1}, respectively) based on PTR-MS measurements at UMBS (Kim et al., 2009). Considering uncertainties and variability, modeled α- and β-pinene emission rates were also in agreement with measured fluxes at UMBS using a disjunct eddy accumulation system (Edwards et al., 2012); these new speciated MT flux measurements by Edwards et al. (2012) will help constrain emissions in future modeling efforts. Comparison between measured (PTR-LIT) and base modeled total MT concentrations ranged from agreement to an under-prediction of up to a factor of ~3; however, these values were still within the range of measured variability (Fig. 2).

3.2 BVOC OH reactivity

Assessment of the total OH reactivity, which is the inverse of the OH lifetime, is indicative of the effective concentration of OH sinks. The specific nature of these sinks provides insights into impacts on ozone, organic nitrates, and secondary organic aerosol formation. Since the efficiency of organic nitrate formation depends on the size of the molecule reacting with OH (Arey et al., 2001), the efficiency of O_3 formation also depends on the particular VOC reactants. During measurements at UMBS in the summer of 2000, Di Carlo et al. (2004) measured total OH reactivity, which was found to range from <1 to ~12 s^{-1} depending on ambient temperature. However, the mean difference between the measured and calculated OH reactivity was 2.6 ± 1.0 s^{-1}, ranging from <0.5 to 3.7 s^{-1} (Di Carlo et al., 2004). Since this “missing” OH reactivity was found to be exponentially dependent on ambient temperature and independent of light, it was suggested that unmeasured reactive BVOCs were the likely source of this "missing" OH reactivity. Of the 57 BVOCs measured during branch-level emission studies at UMBS and included herein, only nine (isoprene, β-myrcene, 1,8-cineole, α-phellandrene, α-pinene, β-pinene, 3-carene, camphene, and limonene) were considered by Di Carlo et al. (2004). Therefore, we examined possible contributions of primary BVOCs that were not included in the Di Carlo et al. (2004) study.

Individual component OH reactivities were calculated as the concentration of a species multiplied by its reaction rate constant with OH. For the base BVOC production scenario in this study, the diurnal variability of the calculated OH reactivity for the 57 modeled BVOCs, plus the major first generation isoprene oxidation products MVK, MACR, IP-HMY, and IP-MHY, ranged from ~0.2–10.4 s^{-1}, depending on the time of day (Fig. 3a), similar to the Di Carlo et al. (2004) study. It should be noted that a similar ambient temperature range was observed in 2000 compared to the modeled 2008. Simulated contributions from isoprene reached a maximum of 92 % during the day with a minimum in the early morning of 7 % for ~12 m above the forest canopy (location of measurements by Di Carlo et al., 2004). The simulated OH reactivity for BVOCs not considered by Di Carlo et al. (2004) was calculated to range from ~0.08–0.31 s^{-1} (0.01–0.86 s^{-1}, considering emissions uncertainties) (Fig. 3b), with the largest contributions from *trans*-ocimene, *cis*-ocimene, γ-terpinene, and sabinene. This suggests that directly emitted BVOCs comprise less than 25 % of the average "missing" OH reactivity measured in 2000. The simulated twenty-four hour integrated BVOC emissions (on a molar basis) were 93 % isoprene, 6 % monoterpenes, 0.5 % sesquiterpenes, and 0.6 % other BVOCs based on detailed branch-level emission rate measurements. Given that the "missing" reactivity described by Di Carlo et al. (2004) was ~33 % of the total, it is therefore logical to conclude that the noted "missing" reactivity could be due primarily to isoprene oxidation products, particularly during mid-day. This is consistent with a recent OH reactivity study attributing "missing" OH reactivity to oxidation products rather than direct emissions (Lou et al., 2010). Recent branch enclosure OH reactivity measurements at UMBS also suggest that the contribution from previously unmeasured BVOC emissions is minimal and that isoprene oxidation products may contribute significantly to the total OH reactivity at UMBS (Kim et al., 2011b). Modeling of the isoprene oxidation products hydroxyacetone, glyoxal, methylglyoxal, and C_4- and C_5-hydroxycarbonyls suggests contributions of ~8 % to the total ambient OH reactivity at UMBS; thus, Kim et al. (2011b) recommended that further generations of isoprene oxidation products should also be examined.

3.3 Biogenic organic nitrates and NO_y budget

Here we define total biogenic organic nitrates as the sum of primary and secondary biogenic organic nitrates, as well as nitrates formed from reaction of first generation isoprene oxidation products (MVK, MACR, IP-HMY, and IP-MHY). At ~12 m above the forest canopy, the simulated concentration of total biogenic organic nitrates ranged from 12–74 ppt (4–137 ppt, considering emissions uncertainties) through the day (Fig. 4). In the morning hours, enhanced vertical mixing transported the $RONO_2$ produced in the near canopy environment upward, resulting in increased [$RONO_2$] aloft (shown for ~560 m). In comparison, the measured NO_y^* (~NO_y-HNO_3) concentration at ~12 m above the forest canopy ranged from ~1.4–4.5 ppb over the course of the average day; during a previous UMBS study, HNO_3 comprised ~30 % of NO_y on average (Thornberry et al., 2001). The fraction of simulated biogenic $RONO_2$/measured NO_y^* ranged from 0.01 at night to 0.04 during the day. When measured total $RONO_2$ and NO_y^* data were both available ($n = 7$) at UMBS for the summer of 2008, the average measured $RONO_2$/NO_y^* ratio was 0.17. Comparison of measured [$RONO_2$] with simulated biogenic [$RONO_2$] suggests that ~2–48 % of the total $RONO_2$ was associated with local biogenic $RONO_2$; the lowest percentages were from the early morning, when transported $RONO_2$ was likely more important (Alaghmand et al., 2011) and when isoprene, and therefore isoprene nitrates, were under-predicted by the model.

During summertime aircraft-based measurements above the Eastern US, Perring et al. (2009a) observed ~18 % of NO_y to be attributed to organic nitrates when isoprene concentrations exceeded 500 ppt in the boundary layer below 0.5 km. Formaldehyde was correlated with the total organic nitrate concentrations, suggesting a major contribution from isoprene (Perring et al., 2009a). For UMBS, the contribution of isoprene-derived organic nitrates to the total simulated biogenic organic nitrates at ~12 m above the forest canopy was predicted to reach a maximum of ~89 % in the afternoon (12:00–17:30) with a minimum of ~20 % in the early morning (05:00 EST), when the contribution from monoterpenes reached its daily maximum (~70 %). The calculated contribution of isoprene-derived organic nitrates to total biogenic organic nitrates was greater than 90 % at all altitudes in the afternoon when vertical mixing and the isoprene nitrate production rate were highest. In the early morning, the fractional contribution of isoprene-derived organic nitrates was simulated to be <40 % below ~150 m, compared to >90 % above ~1400 m. This is due to the relatively greater emissions of monoterpenes at night compared to isoprene, resulting in monoterpene nitrate production in the near-canopy environment. These differences in the vertical profiles of the isoprene and monoterpene nitrates are clearly shown in Fig. 5. Simulated monoterpene nitrate concentrations below ~200 m were higher at night than during the day due to nighttime monoterpene emissions and reaction with NO_3. Above ~200 m, the monoterpene nitrate concentrations were lower at night than during the daytime due to decreased vertical mixing; however, we note uncertainties in the low nighttime mixing as K-theory does not capture nighttime turbulence events that have been observed in stable nocturnal boundary layers (e.g. Mahrt et al., 1998; Salmond and McKendry, 2005).

While simulated primary organic nitrate production at ~12 m reached a maximum in the mid-day (17 times greater than nighttime production), the specific BVOCs and oxidants contributing to organic nitrate production changed with time of day, as shown in Fig. 6. At ~12 m above the forest canopy at night, monoterpene-NO_3 reactions comprised up to 83 % of primary organic nitrate production, with isoprene-OH reactions comprising up to 82 % during the daytime. At night, the major contributors (>5 %) to primary organic nitrate production were predicted to be limonene, γ-terpinene, α-pinene, *cis*-ocimene, β-pinene, sabinene, β-myrcene, and α-farnesene.

Trans-ocimene, a light-dependent monoterpene, was estimated to be the greatest non-isoprene contributor to primary organic nitrate production (up to ∼10 %) during the day through reaction with OH. It is quite noteworthy that during the day (11:00–17:30 EST), ∼8 % of the primary organic nitrate production was predicted to be from isoprene-NO_3 reactions due to high isoprene concentrations (modeled daytime average [isoprene] = 2.82 ppb; modeled daytime average [NO_3] = 0.10 ppt). The NO_3 lifetime versus photolysis was estimated to be ∼5 s, compared to that for reaction with NO or isoprene of ∼18 s and ∼21 s, respectively. Thus, while [NO_3] was lower in the daytime (by ∼4 times on average compared to nighttime), isoprene concentrations were much higher (by ∼45 times, modeled) in the daytime, so these are compensating effects. This led to a greater predicted rate of primary isoprene nitrate production via NO_3 in the daytime (Fig. S5). However, due to under-predicted isoprene concentrations at night (Sect. 3.1), isoprene nitrate production from NO_3 chemistry at night was also likely under-predicted.

The 24 h total column simulated local biogenic $RONO_2$ production rate was calculated to be 18 [8–36] μmol m^{-2} d^{-1}. In comparison, soil measurements at UMBS showed an estimated source NO_x flux of 4.3 μmol m^{-2} d^{-1} (Alaghmand et al., 2011), highlighting the significance of the local formation of organic nitrates. Overall, dry deposition, horizontal advection, and chemical reaction accounted for ∼15 %, ∼52 % and ∼32 %, respectively, of organic nitrate loss in the simulations (Fig. S6). The modeled organic nitrate dry deposition rate of 2.8 [1.2–5.5] μmol m^{-2} d^{-1} agrees with the previous estimate for organic nitrogen dry deposition (2.0 μmol m^{-2} d^{-1}, ∼1 % of the total calculated nitrogen dry deposition) at UMBS by Hill et al. (2005). In this model, horizontal advection removed organic nitrates; however, in the atmosphere, more extensive processing of the organic nitrates occurs as the air mass moves downwind of this BVOC source region. To evaluate the impact of continued oxidation for longer timescales in the downwind plume, a simulation was run with horizontal advection turned off and BVOC emissions only allowed during the first spin-up day in the model with evaluation of the second day. During the second simulation day, the concentration of total simulated biogenic organic nitrates, at ∼12 m above the forest canopy, declined by ∼92 % with an increasing fraction of secondary organic nitrates (59 % to 90 % of the total), showing the impact of reactions with OH, O_3, and NO_3, as well as dry deposition. In particular, since most secondary isoprene nitrates release NO_x upon subsequent reaction (Paulot et al., 2009), the total simulated concentration of isoprene nitrates decreased significantly during this time period, corresponding to a calculated increase in NO_2 of ∼138 ppt. This is equal to ∼11 % of the daily average NO_2 concentration at UMBS.

3.4 Individual isoprene nitrates

Recent laboratory studies by Paulot et al. (2009), Rollins et al. (2009), Lockwood et al. (2010), and Costa (2011) allowed the simulation of individual isoprene nitrate species, shown in Tables 2 and 3, formed via reaction of isoprene with OH or NO_3. In the mid-day at ∼12 m above the forest canopy, ∼91 % of the primary isoprene nitrates were formed via OH oxidation, compared to ∼42 % at night when NO_3 oxidation was prevalent. Previously, Giacopelli et al. (2005), using a zero-dimensional model that did not include NO_3 chemistry, predicted a maximum isoprene nitrate concentration of 79 ppt for UMBS. The most abundant individual isoprene nitrate isomers, at ∼12 m above the forest canopy, in the daytime were predicted here to be $RONO_2$-4,3, estimated to be present at concentrations up to 28 [13–49] ppt, and $RONO_2$-1,2 (up to 10 [5–18] ppt) (Fig. 7, see Table 2 for structures); at their maximum concentrations at this height, these compounds comprised ∼60 % and ∼22 % of the primary isoprene nitrates produced via OH oxidation. These two primary isoprene nitrates are the most abundantly produced nitrates via OH oxidation at relative yields of 63.0 % and 18.3 %, respectively, as observed by Costa (2011). The enrichment in $RONO_2$-1,2 relative to its yield was due to lower predicted reaction rates with OH and O_3 compared to $RONO_2$-4,3 (Table 2). Through the night, the relative concentrations of the primary OH-produced isoprene nitrates changed due to reaction with NO_3. For example, at 04:30 EST, the relative concentrations of $RONO_2$-4,3, $RONO_2$-3,4, $RONO_2$-1,2, $RONO_2$-2,1, $RONO_2$-4,1, and $RONO_2$-1,4 were 38 %, 1 %, 47 %, 13 %, 1 %, and 0.2 %, respectively. $RONO_2$-1,2, in particular, was significantly enriched compared to its relative production yield due to a lower predicted reaction (removal) rate with NO_3, compared to the other nitrates (Table 2). During previous measurements at UMBS, Grossenbacher et al. (2001) and Giacopelli et al. (2005) detected two gas chromatographic peaks associated with nitrates produced from the OH-oxidation of isoprene, with associated average diurnal concentrations ranging from ~1–10 ppt and observations up to ~90 ppt; based on recent studies (Costa, 2011), we believe these peaks correspond to the $RONO_2$-4,3 and $RONO_2$-1,2 species, eluting in that order.

Reaction of primary isoprene nitrates with OH, O_3, or NO_3 can produce secondary isoprene nitrates, as described by Giacopelli et al. (2005), Paulot et al. (2009), and Rollins et al. (2009) (Table 3); in addition, nitrates can form from subsequent oxidation of the first generation isoprene oxidation products, including MVK, MACR, and the C_5-unsaturated hydroxyaldehyde isomers (Paulot et al., 2009; Costa, 2011). In general, the contributions of secondary isoprene nitrates and nitrates formed from first generation isoprene oxidation products were simulated to increase with altitude and time of day. Following initiation of isoprene emissions in the morning, primary isoprene nitrates contributed ~90 % of the total simulated concentration of isoprene nitrates (defined here as primary, secondary, and first generation oxidation product isoprene nitrates) at ~12 m above the forest canopy (Fig. 7). Through the day and overnight, secondary isoprene nitrate concentrations increased due to reactions of first generation isoprene oxidation products and primary isoprene nitrates. By early morning, the secondary isoprene nitrates and nitrates formed from the reaction of first generation isoprene oxidation products contribute ~55 % and ~15 %, respectively, to the total simulated isoprene nitrate concentration at ~12 m above the forest canopy.

3.5 Monoterpene nitrates

Monoterpenes accounted for ~6 % of the simulated BVOC emissions (on a molar basis) at UMBS. At night, simulated monoterpenes comprised ~80–82 % of the total BVOC emissions at UMBS (Fig. S3). The individual monoterpenes α-pinene, limonene, β-pinene, γ-terpinene, β-myrcene, *cis*-ocimene, and sabinene each comprised >5 % of

Title Page
Abstract Introduction
Conclusions References
Tables Figures
◄◄ ►►
◄ ►
Back Close
Full Screen / Esc
Printer-friendly Version
Interactive Discussion

the nighttime total BVOC emissions. Unlike isoprene concentrations, which reached a maximum in the mid-day for ∼12 m above the forest canopy, the measured average total monoterpene concentration only varied by a factor of ∼2 through the entire day (119–245 ppt) (Fig. 2). While significant uncertainties exist with respect to the $RONO_2$ yields of numerous monoterpenes, as noted in section 2, the trends in the simulated temporal and vertical profiles of monoterpene nitrates can be examined (Fig. 8). In contrast to the diurnal cycle of isoprene nitrates (Fig. 7), the maximum concentrations of primary and secondary monoterpene nitrates at ∼12 m above the forest canopy occured at night due to the reaction of monoterpenes with NO_3 (Figures 6 and 8). Compared to isoprene, most monoterpenes are characterized by higher rate constants for reaction with NO_3 and lower rate constants for reaction with OH; when coupled with higher $RONO_2$ yields for reaction with NO_3 compared to OH (Table 1), this results in the nighttime maximum for ∼12 m above the forest canopy. However, similar to isoprene, the concentration of monoterpene nitrates aloft was governed by vertical mixing with a maximum in the afternoon. As shown in Fig. 8, significant precursors to monoterpene nitrates included limonene (both OH and NO_3 reactions), γ-terpinene (NO_3 reaction), α-pinene (both OH and NO_3 reactions), β-pinene (both OH and NO_3 reactions), and *trans*-ocimene (OH reaction).

3.6 Impacts of forest succession on BVOC emissions and organic nitrates

A major fraction of the upper Great Lakes region forest consists of aspen trees (*Populus grandidentata* and *Populus tremuloides*), which grew following the harvest of mature forests in the late 19th and early 20th centuries (Friedman and Reich, 2005). Given the short lifetimes (<100 yr) of aspen trees, the forest in Northern Michigan is undergoing forest succession, where the aspen trees are currently being replaced by northern hardwoods (*Acer rubrum, Acer saccharum, Fagus grandifola*) and upland pine (*Pinus strobus, Pinus resinosa*) (Bergen and Dronova, 2007). Here, we simulated the effect of these future forest emissions on organic nitrate composition using current (summer 2008) temperatures. Two future forest composition scenarios were simulated with aspen being replaced by either northern hardwoods or upland pine (see supporting information for more detail).

At UMBS, isoprene is emitted primarily by aspen and red oak, such that loss of aspen trees decreased simulated isoprene emissions by 46–53 % to a mid-day average flux of 1.1–1.3 $\text{mg C m}^{-2}\,\text{h}^{-1}$ (1.1–1.3 × 10^{19} $\text{molecules m}^{-2}\,\text{h}^{-1}$). The replacement of the aspen by northern hardwoods and upland pine changed total monoterpene, sesquiterpene, and other BVOC emissions by factors of 0.7–1.5, 1.5–1.8, and 1.0–2.0, respectively. Corresponding mid-day average fluxes of monoterpenes and sesquiterpenes were predicted to be 0.2–0.3 $\text{mg m}^{-2}\,\text{h}^{-1}$ and 0.04 $\text{mg m}^{-2}\,\text{h}^{-1}$, respectively, such that isoprene emissions were predicted to still comprise 83–89 % of the total BVOC emissions at UMBS (compared to the current 93 %). The composition of the BVOC emissions was also predicted to change (Fig. S7), where replacement of aspen with either northern hardwoods or upland pines increased several sesquiterpenes (α-cedrene, α-muurolene, γ-muurolene, γ-cadinene, β-bisabolene β-farnesene, and α-humulene) by factors of more than 10; replacement with northern hardwoods was also predicted to increase emission rates of certain monoterpenes (4-carene, p-cymenene, and cyclofenchone) and oxygenated BVOCs (1,8-cineole, cis-linalool oxide, trans-linalool oxide, camphene, borneol) by factors of more than 10. Under both northern hardwood and upland pine future forest scenarios, α-pinene, β-pinene, limonene, and β-myrcene were predicted to each contribute greater than 5 % to the total BVOC emissions at night.

Isoprene was predicted to reach an afternoon maximum concentration of ~2 ppb at ~12 m above the forest canopy, compared to current predicted maximum of ~3.6 ppb (base production scenarios). Average daily total monoterpene, sesquiterpene, and other BVOC concentrations, at ~12 m above the forest canopy, ranged from approximately 89–153, 8–9, and 23–40 ppt, respectively (compared to ~92, 5, and 19 ppt, respectively, for the current simulations). Due to the reduced isoprene concentrations, and therefore reduced total BVOC concentrations, the total biogenic organic nitrate concentration was predicted to decrease in the afternoon by 35–40 % at ~12 m above the forest canopy. While isoprene nitrate concentrations were predicted to decrease by ∼46 %, the concentrations of organic nitrate derived from monoterpenes, sesquiterpenes, and other BVOCs increased in the late afternoon by factors of ∼4–5, 2–3, 6–11, respectively. These are likely lower limit changes for the monoterpenes and their oxidation products, as it does not take into account other climate changes, such as increasing ambient temperatures and elevated CO_2 (Peñuelas and Staudt, 2010).

4 Conclusions

The fate of the 57 individual BVOCs locally emitted from the mixed forest in Northern Michigan and their role in organic nitrate formation in the lower troposphere was investigated. In order to obtain a first estimate of detailed organic nitrate formation from speciated compounds, atmospheric processes were simplified; however, agreement was observed between modeled and measured primary BVOC concentrations above the canopy. BVOC emission rates are difficult to determine due to tree-to-tree variability and sampling challenges during branch enclosure BVOC emission measurements (e.g. Ortega et al., 2008), leading to large ranges in estimated production rates, shown here to result in a range of oxidation product concentrations. In the future, improved canopy-level flux measurements of speciated monoterpenes, such as those recently completed by Edwards et al. (2012) at UMBS, will improve modeling of individual monoterpenes at the canopy level. The question of “missing” OH reactivity (Di Carlo et al., 2004) was examined by modeling the OH reactivity of the 57 BVOCs and first generation isoprene oxidation products. Approximately 25 % of the “missing” OH reactivity can be attributed to direct BVOC emissions. However, given the high isoprene emission rates, isoprene oxidation products (many of which have not been measured) likely comprise a significant portion of the OH reactivity. This is in agreement with the conclusions by Kim et al. (2011b) and is an effect worthy of further examination via quantification of multiple generations of isoprene oxidation products.

During the daytime at ~12 m above the forest canopy, simulated isoprene-OH reactions comprised up to 82 % of simulated primary organic nitrate production. In the afternoon, when vertical mixing and isoprene nitrate production were highest, the simulated contribution of isoprene-derived organic nitrates was greater than 90 % at all altitudes, with the concentration of secondary isoprene nitrates increasing with altitude. In addition, NO_3 reactions led to high simulated fractions of primary isoprene nitrates, ranging from ~9 % during mid-day at ~12 m above the forest canopy to ~58 % at night; thus, the individual products and fates of isoprene-NO_3 reactions need to be studied in detail to expand upon the work of Perring et al. (2009b) and Rollins et al. (2009) and improve our understanding of this pathway. In general, the contributions of secondary isoprene nitrates and nitrates formed from first generation isoprene oxidation products increased with altitude and time of day; however, the formation and removal of these species are poorly understood due to few studies and should be the focus of future laboratory investigations.

At ~12 m above the forest canopy, simulated monoterpene-NO_3 reactions comprised up to ~83 % of primary organic nitrate production at night, resulting in major contributions to the total simulated biogenic $RONO_2$ in the early morning. In particular, the formation of organic nitrates from reactions of γ-terpinene, limonene, α-pinene, *cis*-ocimene, sabinene, β-pinene, and isoprene with NO_3 each contributed greater than 5 % to the total simulated biogenic organic nitrate production at night. However, the organic nitrate yields for reactions of NO_3 with many significant BVOC precursors, including γ-terpinene, sabinene, *cis*-ocimene, α-thujene, and β-myrcene, have not been measured, lending uncertainty to the simulations. Also, the rate constants corresponding to the reactions of α-thujene and α-farnesene with NO_3 have not been measured, and these reactions are estimated to contribute up to ~3 % and ~5 %, respectively, of primary organic nitrate production each at night at ~12 m above the forest canopy. Likewise, the NO_3 reaction rate constants have not been measured for most sesquiterpenes and oxygenated BVOCs emitted at UMBS. The contribution of NO_3 reactions to the formation of isoprene nitrates and terpene nitrates is expected to be even greater in the Southeastern US, which is impacted by higher BVOC emissions and higher NO_x concentrations, similar to the observations for OH-produced isoprene nitrates (Grossenbacher et al., 2004). In addition, laboratory experiments should focus on detailed studies of organic nitrates formed via reactions of limonene with NO_3, γ-terpinene with NO_3, and *trans*-ocimene with OH given their predicted significant contribution to total organic nitrates. Further, forest succession was predicted to lead to significantly increased afternoon concentrations of monoterpene-derived organic nitrates, underscoring the need to better understand the formation and fate of these species, which can lead to secondary organic aerosol formation (e.g. Fry et al., 2009; Rollins et al., 2009; Fry et al., 2011).

Organic nitrates serve as reservoirs of NO_x, impacting ozone production (both locally and downwind) (e.g. Wu et al., 2007), the oxidative capacity of the atmosphere (impacting trace gas removal, secondary organic aerosol formation and processing) (e.g. Rollins et al., 2010), and nitrogen availability to ecosystems (Lockwood et al., 2008). Since horizontal advection accounted for ~52 % of nitrate loss in the simulations, the local formation of biogenic $RONO_2$ is expected to impact downwind atmospheric chemistry and deposition processes; estimates suggested significant NO_2 release downwind, due to decreases in isoprene nitrate concentrations alone over the course of one day of transport. The relative concentrations of OH-produced primary isoprene nitrates changed significantly at night depending on their removal rates via reaction with NO_3, the rate constants for which were calculated to span a large range, from 4.56×10^{-14} to $4.81 \times 10^{-12}\,\mathrm{cm^3\,molec^{-1}\,s^{-1}}$ (Pfrang et al., 2006). These rate constants need to be measured to verify and improve the prediction of this nighttime removal. However, since the speciated isoprene nitrates have been measured in the laboratory, and in some cases in the field, it should be possible to achieve closure on the total $RONO_2$ budget at this isoprene-dominated site, given the major contributions of isoprene nitrates to the total simulated biogenic $[RONO_2]$ at UMBS. Given the relatively low measured NO_x conditions at UMBS (average [NO] = 67 ppt; average $[NO_2]$ = 1.2 ppb), and therefore low propensity toward organic nitrate formation, the formation and downwind transport of biogenic organic nitrates formed in areas of higher NO_x emissions (e.g. Southeastern US (Fiore et al., 2005)) are expected to significantly impact downwind atmospheric composition.

Supplementary material related to this article is available online at: http://www.atmos-chem-phys-discuss.net/12/17031/2012/ acpd-12-17031-2012-supplement.pdf.

Acknowledgements. Funding was provided by the National Science Foundation (AGS-0904151 and AGS-0542701) and Environmental Protection Agency (STAR grant R833750). K. A. Pratt gratefully acknowledges a NOAA climate and global change postdoctoral fellowship, administered by UCAR. L. H. Mielke acknowledges a NSF-IGERT fellowship for biosphere/atmosphere research training. M. A. Carroll (University of Michigan) and S. Bertman (Western Michigan University) are thanked for temperature and ozone data. J. Fuentes (Pennsylvania State University) is acknowledged for discussions. This is publication #1143 of the Purdue Climate Change Research Center.

References

Alaghmand, M., Shepson, P. B., Starn, T. K., Jobson, B. T., Wallace, H. W., Carroll, M. A., Bertman, S. B., Lamb, B., Edburg, S. L., Zhou, X., Apel, E., Riemer, D., Stevens, P., and Keutsch, F.: The Morning NO_x maximum in the forest atmosphere boundary layer, Atmos. Chem. Phys. Discuss., 11, 29251–29282, doi:10.5194/acpd-11-29251-2011, 2011.

Arey, J., Aschmann, S. M., Kwok, E. S. C., and Atkinson, R.: Alkyl nitrate, hydroxy nitrate, and hydroxycarbonyl formation from the NO_x-air photooxidations of C_5–C_8 *n*-alkanes, J. Phys. Chem. A, 105, 1020–1027, 2001.

Atkinson, R. and Arey, J.: Atmospheric degradation of volatile organic compounds, Chem. Rev., 103, 4605–4638, 2003a.

Atkinson, R. and Arey, J.: Gas-phase tropospheric chemistry of biogenic volatile organic compounds: a review, Atmos. Environ., 37, S197–S219, 2003b.

Atkinson, R., Hasegawa, J., and Aschmann, S. M.: Rate constants for the gas-phase reactions of O_3 with a series of monoterpenes and related compounds at 296 ± 2 K, Int. J. Chem. Kinet., 22, 871–887, 1990.

Atkinson, R., Arey, J., Aschmann, S. M., Corchnoy, S. B., and Shu, Y.: Rate constants for the gas-phase reactions of *cis*-3-hexen-1-ol, *cis*-3-hexenylacetate, *trans*-2-hexenal, and linalool with OH and NO_3 radicals and O_3 at 296 ± 2 K, and OH radical formation yields from the O_3 reactions, Int. J. Chem. Kinet., 27, 941–955, 1995.

Atkinson, R., Baulch, D. L., Cox, R. A., Crowley, J. N., Hampson, R. F., Hynes, R. G., Jenkin, M. E., Rossi, M. J., Troe, J., and IUPAC Subcommittee: Evaluated kinetic and photochemical data for atmospheric chemistry: Volume II – gas phase reactions of organic species, Atmos. Chem. Phys., 6, 3625–4055, doi:10.5194/acp-6-3625-2006, 2006.

Barket, D. J., Grossenbacher, J. W., Hurst, J. M., Shepson, P. B., Olszyna, K., Thornberry, T., Carroll, M. A., Roberts, J., Stroud, C., Bottenheim, J., and Biesenthal, T.: A study of the NO_x dependence of isoprene oxidation, J. Geophys. Res., 109, D11310, doi:10.1029/2003JD003965, 2004.

Beaver, M. R., Clair, J. M. St., Paulot, F., Spencer, K. M., Crounse, J. D., LaFranchi, B. W., Min, K. E., Pusede, S. E., Wooldridge, P. J., Schade, G. W., Park, C., Cohen, R. C., and Wennberg, P. O.: Importance of biogenic precursors to the budget of organic nitrates: observations of multifunctional organic nitrates by CIMS and TD-LIF during BEARPEX 2009, Atmos. Chem. Phys., 12, 5773–5785, doi:10.5194/acp-12-5773-2012, 2012.

Bergen, K. M. and Dronova, I.: Observing succession on aspen-dominated landscapes using a remote sensing-ecosystem approach, Landscape Ecol., 22, 1395–1410, 2007.

Bollinger, M. J., Sievers, R. E., Fahey, D. W., and Fehsenfeld, F. C.: Conversion of nitrogen dioxide, nitric acid, and *n*-propyl nitrate to nitric oxide by gold-catalyzed reduction with carbon monoxide, Anal. Chem., 55, 1980–1986, 1983.

Bouvier-Brown, N. C., Goldstein, A. H., Gilman, J. B., Kuster, W. C., and de Gouw, J. A.: In-situ ambient quantification of monoterpenes, sesquiterpenes, and related oxygenated compounds during BEARPEX 2007: implications for gas- and particle-phase chemistry, Atmos. Chem. Phys., 9, 5505–5518, doi:10.5194/acp-9-5505-2009, 2009.

Boy, M., Sogachev, A., Lauros, J., Zhou, L., Guenther, A., and Smolander, S.: SOSA – a new model to simulate the concentrations of organic vapours and sulphuric acid inside the ABL – Part 1: Model description and initial evaluation, Atmos. Chem. Phys., 11, 43–51, doi:10.5194/acp-11-43-2011, 2011.

Brown, S. S., deGouw, J. A., Warneke, C., Ryerson, T. B., Dubé, W. P., Atlas, E., Weber, R. J., Peltier, R. E., Neuman, J. A., Roberts, J. M., Swanson, A., Flocke, F., McKeen, S. A., Brioude, J., Sommariva, R., Trainer, M., Fehsenfeld, F. C., and Ravishankara, A. R.: Nocturnal isoprene oxidation over the Northeast United States in summer and its impact on reactive nitrogen partitioning and secondary organic aerosol, Atmos. Chem. Phys., 9, 3027–3042, doi:10.5194/acp-9-3027-2009, 2009.

Bryan, A. M., Bertman, S. B., Carroll, M. A., Dusanter, S., Edwards, G. D., Forkel, R., Griffith, S., Guenther, A. B., Hansen, R. F., Helmig, D., Jobson, B. T., Keutsch, F. N., Lefer, B. L., Pressley, S. N., Shepson, P. B., Stevens, P. S., and Steiner, A. L.: In-canopy gas-phase chemistry during CABINEX 2009: sensitivity of a 1-D canopy model to vertical mixing and isoprene chemistry, Atmos. Chem. Phys. Discuss., 12, 12801–12852, doi:10.5194/acpd-12-12801-2012, 2012.

Carroll, M. A., Bertman, S. B., and Shepson, P. B.: Overview of the program for research on oxidants: photochemistry, emissions, and transport (PROPHET) summer 1998 measurements intensive, J. Geophys. Res., 106, 24275–24288, 2001.

Carter, W. P. L. and Atkinson, R.: Development and evaluation of a detailed mechanism for the atmospheric reactions of isoprene and NO_x, Int. J. Chem. Kinet., 28, 497–530, 1996.

Chen, X., Hulbert, D., and Shepson, P. B.: Measurement of the organic nitrate yield from OH reaction with isoprene, J. Geophys. Res., 103, 25563–25568, 1998.

Chuong, B. and Stevens, P. S.: Measurements of the kinetics of the OH-initiated oxidation of isoprene, J. Geophys. Res., 107, 4162, doi:10.1029/2001JD000865, 2002.

Corchnoy, S. B. and Atkinson, R.: Kinetics of the gas-phase reactions of OH and NO_3 radicals with 2-carene, 1,8-cineole, *p*-cymene, and terpinolene, Environ. Sci. Technol., 24, 1497–1502, 1990.

Costa, A. W.: Coupling Between the Carbon and Nitrogen Cycles in a Forested Environment, Ph.D., Chemistry, Purdue University, West Lafayette, IN, 279 pp., 2011.

Davis, M. E., Tapscott, C., and Stevens, P. S.: Measurements of the kinetics of the OH-initiated oxidation of β-pinene: radical propogation in the OH + β-pinene + O_2 + NO reaction system, Int. J. Chem. Kinet., 37, 522–531, 2005.

Day, D. A., Wooldridge, P. J., Dillon, M. B., Thornton, J. A., and Cohen, R. C.: A thermal dissociation laser-induced fluorescence instrument for in situ detection of NO_2, peroxy nitrates, alkyl nitrates, and HNO_3, J. Geophys. Res., 107, 4046, doi:10.1029/2001JD000779, 2002.

Day, D. A., Dillon, M. B., Wooldridge, P. J., Thornton, J. A., Rosen, R. S., Wood, E. C., and Cohen, R. C.: On alkyl nitrates, O_3, and the “missing NO_y”, J. Geophys. Res., 108, 4501, doi:10.1029/2003JD003685, 2003.

Di Carlo, P., Brune, W. H., Martinez, M., Harder, H., Lesher, R., Ren, X., Thornberry, T., Carroll, M. A., Young, V., Shepson, P. B., Riemer, D., Apel, E., and Campbell, C.: Missing OH reactivity in a forest: evidence for unknown reactive biogenic VOCs, Science, 304, 722–725, 2004.

Dusanter, S., Vimal, D., Stevens, P. S., Volkamer, R., and Molina, L. T.: Measurements of OH and HO_2 concentrations during the MCMA-2006 field campaign – Part 1: Deployment of the Indiana University laser-induced fluorescence instrument, Atmos. Chem. Phys., 9, 1665–1685, doi:10.5194/acp-9-1665-2009, 2009.

Edwards, G. D., Martins, D. K., Starn, T., Pratt, K., and Shepson, P. B.: A disjunct eddy accumulation system for the measurement of BVOC fluxes: instrument characterizations and field deployment, Atmos. Meas. Tech. Discuss., 5, 2703–2746, doi:10.5194/amtd-5-2703-2012, 2012.

Espada, C. and Shepson, P. B.: The production of organic nitrates from atmospheric oxidation of ethers and glycol ethers, Int. J. Chem. Kinet., 37, 686–699, 2005.

Espada, C., Grossenbacher, J. W., Ford, K., Couch, T., and Shepson, P. B.: The production of organic nitrates from various anthropogenic volatile organic compounds, Int. J. Chem. Kinet., 37, 675–685, 2005.

Faloona, I., Tan, D., Brune, W., Hurst, J., Barket, D., Couch, T. L., Shepson, P., Apel, E., Riemer, D., Thornberry, T., Carroll, M. A., Sillman, S., Keeler, G. J., Sagady, J., Hooper, D., and Paterson, K.: Nighttime observations of anomalously high levels of hydroxyl radicals above a deciduous forest canopy, J. Geophys. Res., 106, 24315–24333, 2001.

Farmer, D. K. and Cohen, R. C.: Observations of HNO_3, ΣAN, ΣPN, and NO_2 fluxes: evidence for rapid HO_x chemistry within a pine forest canopy, Atmos. Chem. Phys., 8, 3899–3917, doi:10.5194/acp-8-3899-2008, 2008.

Fiore, A. M., Horowitz, L. W., Purves, D. W., Levy, H., Evans, M. J., Wang, Y., Li, Q., and Yantosca, R. M.: Evaluating the contribution of changes in isoprene emissions to surface ozone trends over the Eastern US, J. Geophys. Res., 110, D12303, doi:10.1029/2004JD005485, 2005.

Forkel, R., Siedl, W., Dlugi, R., and Deigele, E.: A one-dimensional numerical model to simulate formation and balance of sulfate during radiation fog events, J. Geophys. Res., 95, 18501–18515, 1990.

Forkel, R., Klemm, O., Graus, M., Rappenglück, B., Stockwell, W. R., Grabmer, W., Held, A., Hansel, A., and Steinbrecher, R.: Trace gas exchange and gas phase chemistry in a Norway spruce forest: a study with a coupled 1-dimensional canopy atmospheric chemistry emission model, Atmos. Environ., 40, 28–42, 2006.

Friedman, S. K. and Reich, P. B.: Regional legacies of logging: departure from presettlement forest conditions in Northern Minnesota, Ecol. Appl., 15, 726–744, 2005.

Fry, J. L., Kiendler-Scharr, A., Rollins, A. W., Wooldridge, P. J., Brown, S. S., Fuchs, H., Dubé, W., Mensah, A., dal Maso, M., Tillmann, R., Dorn, H.-P., Brauers, T., and Cohen, R. C.: Organic nitrate and secondary organic aerosol yield from NO_3 oxidation of β-pinene evaluated using a gas-phase kinetics/aerosol partitioning model, Atmos. Chem. Phys., 9, 1431–1449, doi:10.5194/acp-9-1431-2009, 2009.

Fry, J. L., Kiendler-Scharr, A., Rollins, A. W., Brauers, T., Brown, S. S., Dorn, H.-P., Dubé, W. P., Fuchs, H., Mensah, A., Rohrer, F., Tillmann, R., Wahner, A., Wooldridge, P. J., and Cohen, R. C.: SOA from limonene: role of NO_3 in its generation and degradation, Atmos. Chem. Phys., 11, 3879–3894, doi:10.5194/acp-11-3879-2011, 2011.

Fuchs, H., Bohn, B., Hofzumahaus, A., Holland, F., Lu, K. D., Nehr, S., Rohrer, F., and Wahner, A.: Detection of HO_2 by laser-induced fluorescence: calibration and interferences from RO_2 radicals, Atmos. Meas. Tech., 4, 1209–1225, doi:10.5194/amt-4-1209-2011, 2011.

Ganzeveld, L., Eerdekens, G., Feig, G., Fischer, H., Harder, H., Königstedt, R., Kubistin, D., Martinez, M., Meixner, F. X., Scheeren, H. A., Sinha, V., Taraborrelli, D., Williams, J., Vilà-Guerau de Arellano, J., and Lelieveld, J.: Surface and boundary layer exchanges of volatile organic compounds, nitrogen oxides and ozone during the GABRIEL campaign, Atmos. Chem. Phys., 8, 6223–6243, doi:10.5194/acp-8-6223-2008, 2008.

Gao, W., Wesely, M. L., and Dosky, P. V.: Numerical modeling of the turbulent-diffusion and chemistry of NO_x, O_3, isoprene, and other reactive trace gases in and above a forest canopy, J. Geophys. Res., 98, 18339–18353, 1993.

Geyer, A. and Stutz, J.: The vertical structure of $OH–HO_2–RO_2$ chemistry in the noctural boundary layer: a one-dimensional study, J. Geophys. Res., 109, D16301, doi:10.1029/2003JD004425, 2004a.

Geyer, A. and Stutz, J.: Vertical profiles of NO_3, N_2O_5, O_3, and NO_x in the noctural boundary layer: 2. Model studies on the altitude dependence of composition and chemistry, J. Geophys. Res., 109, D12307, doi:10.1029/2003JD004211, 2004b.

Giacopelli, P., Ford, K., Espada, C., and Shepson, P. B.: Comparison of the measured and simulated isoprene nitrate distributions above a forest canopy, J. Geophys. Res., 110, D01304, doi:10.1029/2004JD005123, 2005.

Goldstein, A. H. and Galbally, I. E.: Known and unexplored organic constituents in the Earth's atmosphere, Environ. Sci. Technol., 41, 1514–1521, 2007.

Grossenbacher, J. W., Couch, T., Shepson, P. B., Thornberry, T., Witmer-Rich, M., Carroll, M. A., Faloona, I., Tan, D., Brune, W., Ostling, K., and Bertman, S.: Measurements of isoprene nitrates above a forest canopy, J. Geophys. Res., 106, 24429–24438, 2001.

Grossenbacher, J. W., Barket, D. J., Shepson, P. B., Carroll, M. A., Olszyna, K., and Apel, E.: A comparison of isoprene nitrate concentrations at two forest-impacted sites, J. Geophys. Res., 109, D11311, doi:10.1029/2003JD003966, 2004.

Guenther, A., Hewitt, C. N., Erickson, D., Fall, R., Geron, C., Graedel, T., Harley, P., Klinger, L., Lerdau, M., McKay, W. A., Pierce, T., Scholes, B., Steinbrecher, R., Tallamraju, R., Taylor, J., and Zimmerman, P.: A global model of natural volatile organic compound emissions, J. Geophys. Res., 100, 8873–8892, 1995.

Guenther, A., Baugh, B., Brasseur, G., Greenberg, J., Harley, P., Klinger, L., Serça, D., and Vierling, L.: Isoprene emission estimates and uncertainties for the Central African EXPRESSO study domain, J. Geophys. Res., 104, 30625–30639, 1999.

Guenther, A. B., Monson, R. K., and Fall, R.: Isoprene and monoterpene emission rate variability: observations with eucalyptus and emission rate algorithm development, J. Geophys. Res., 96, 10799–10808, 1991.

Guenther, A. B., Zimmerman, P. R., Harley, P. C., Monson, R. K., and Fall, R.: Isoprene and monoterpene emission rate variability: model evaluations and sensitivity analyses, J. Geophys. Res., 98, 12609–12617, 1993.

Hallquist, M., Wängberg, I., Ljungström, E., Barnes, I., and Becker, K.-H.: Aerosol and product yields from NO_3 radical-initiated oxidation of selected monoterpenes, Environ. Sci. Technol., 33, 553–559, 1999.

Hauglustaine, D. A., Madronich, S., Ridley, B. A., Walega, J. G., Cantrell, C. A., Shetter, R. E., and Hübler, G.: Observed and model-calculated photostationary state at Mauna Loa Observatory during MLOPEX 2, J. Geophys. Res., 101, 14681–14696, 1996.

Hill, K. A., Shepson, P. B., Galbavy, E. S., and Anastasio, C.: Measurement of wet deposition of inorganic and organic nitrogen in a forest environment, J. Geophys. Res., 110, G02010, doi:10.1029/2005JG000030, 2005.

Hofzumahaus, A., Rohrer, F., Lu, K., Bohn, B., Brauers, T., Chang, C.-C., Fuchs, H., Holland, F., Kita, K., Kondo, Y., Li, X., Lou, S., Shao, M., Zeng, L., Wahner, A., and Zhang, Y.: Amplified trace gas removal in the troposphere, Science, 324, 1702–1704, 2009.

Horowitz, L. W., Fiore, A. M., Milly, G. P., Cohen, R. C., Perring, A., Wooldridge, P. J., Hess, P. G., Emmons, L. K., and Lamarque, J.-F.: Observational constraints on the chemistry of isoprene nitrates over the Eastern US, J. Geophys. Res., 112, D12S08, doi:10.1029/2006JD007747, 2007.

Hurst, J. M., Barket, D. J., Herrera-Gomez, O., Couch, T. L., Shepson, P. B., Faloona, I., Tan, D., Brune, W., Westberg, H., Lamb, B., Biesenthal, T., Young, V., Goldstein, A., Munger, J. W., Thornberry, T., and Carroll, M. A.: Investigation of the nighttime decay of isoprene, J. Geophys. Res., 106, 24335–24346, 2001.

Jones, B. T. and Ham, J. E.: α-terpineol reactions with the nitrate radical: rate constant and gas-phase products, Atmos. Environ., 42, 6689–6698, 2008.

Kerdouci, J., Picquet-Varrault, B., and Doussin, J. F.: Prediction of rate constants for gas-phase reactions of nitrate radical with organic compounds: a new structure-activity relationship, Chem. Phys. Chem., 11, 3909–3920, 2010.

Kim, S., Karl, T., Helmig, D., Daly, R., Rasmussen, R., and Guenther, A.: Measurement of atmospheric sesquiterpenes by proton transfer reaction-mass spectrometry (PTR-MS), Atmos. Meas. Tech., 2, 99–112, doi:10.5194/amt-2-99-2009, 2009.

Kim, D., Stevens, P. S., and Hites, R. A.: Rate constants for the gas-phase reactions of OH and O_3 with β-ocimene, β-myrcene, and α- and β-farnesene as a function of temperature, J. Phys. Chem. A, 115, 500–506, 2011a.

Kim, S., Guenther, A., Karl, T., and Greenberg, J.: Contributions of primary and secondary biogenic VOC tototal OH reactivity during the CABINEX (Community Atmosphere-Biosphere INteractions Experiments)-09 field campaign, Atmos. Chem. Phys., 11, 8613–8623, doi:10.5194/acp-11-8613-2011, 2011b.

Leungsakul, S., Jeffries, H. E., and Kamens, R. M.: A kinetic mechanism for prediting secondary aerosol formation from the reactions of *d*-limonene in the presence of oxides of nitrogen and natural sunlight, Atmos. Environ., 39, 7063–7082, 2005.

Lockwood, A. L., Filley, T. R., Rhodes, D., and Shepson, P. B.: Foliar uptake of atmospheric organic nitrates, Geophys. Res. Lett., 35, L15809, doi:10.1029/2008GL034714, 2008.

Lockwood, A. L., Shepson, P. B., Fiddler, M. N., and Alaghmand, M.: Isoprene nitrates: preparation, separation, identification, yields, and atmospheric chemistry, Atmos. Chem. Phys., 10, 6169–6178, doi:10.5194/acp-10-6169-2010, 2010.

Lou, S., Holland, F., Rohrer, F., Lu, K., Bohn, B., Brauers, T., Chang, C. C., Fuchs, H., Häseler, R., Kita, K., Kondo, Y., Li, X., Shao, M., Zeng, L., Wahner, A., Zhang, Y., Wang, W., and Hofzumahaus, A.: Atmospheric OH reactivities in the Pearl River Delta – China in summer 2006: measurement and model results, Atmos. Chem. Phys., 10, 11243–11260, doi:10.5194/acp-10-11243-2010, 2010.

Mahrt, L., Sun, J., Blumen, W., Delany, T., and Oncley, S.: Nocturnal boundary-layer regimes, Bound-Lay. Meteorol., 88, 255–278, 1998.

Makar, P. A., Fuentes, J. D., Wang, D., Staebler, R. M., and Wiebe, H. A.: Chemical processing of biogenic hydrocarbons within and above a temperate deciduous forest, J. Geophys. Res., 104, 3581–3603, 1999.

Mielke, L. H., Erickson, D. E., McLuckey, S. A., Müller, M., Wisthaler, A., Hansel, A., and Shepson, P. B.: Development of a proton-transfer reaction-linear ion trap mass spectrometer for quantitative determination of volatile organic compounds, Anal. Chem., 80, 8171–8177, 2008.

Mielke, L. H., Pratt, K. A., Shepson, P. B., McLuckey, S. A., Wisthaler, A., and Hansel, A.: Quantitative determination of biogenic volatile organic compounds in the atmosphere using proton-transfer reaction linear ion trap mass spectrometry, Anal. Chem., 82, 7952–7957, 2010.

Mihele, C. M. and Hastie, D. R.: Radical chemistry at a forested continental site: results from the PROPHET 1997 campaign, J. Geophys. Res., 108, 4450, doi:10.1029/2002JD002888, 2003.

Mogensen, D., Smolander, S., Sogachev, A., Zhou, L., Sinha, V., Guenther, A., Williams, J., Nieminen, T., Kajos, M. K., Rinne, J., Kulmala, M., and Boy, M.: Modelling atmospheric OH-reactivity in a boreal forest ecosystem, Atmos. Chem. Phys., 11, 9709–9719, doi:10.5194/acp-11-9709-2011, 2011.

Muthuramu, K., Shepson, P. B., and O'Brien, J. M.: Preparation, analysis, and atmospheric production of multifunctional organic nitrates, Environ. Sci. Technol., 27, 1117–1124, 1993.

Ng, N. L., Chhabra, P. S., Chan, A. W. H., Surratt, J. D., Kroll, J. H., Kwan, A. J., McCabe, D. C., Wennberg, P. O., Sorooshian, A., Murphy, S. M., Dalleska, N. F., Flagan, R. C., and Seinfeld, J. H.: Effect of NO_x level on secondary organic aerosol (SOA) formation from the photooxidation of terpenes, Atmos. Chem. Phys., 7, 5159–5174, doi:10.5194/acp-7-5159-2007, 2007.

Nozière, B., Barnes, I., and Becker, K.-H.: Product study and mechanisms of the reactions of α-pinene and of pinonaldehyde with OH radicals, J. Geophys. Res., 104, 23645–23656, 1999.

O'Brien, J. M., Shepson, P. B., Muthuramu, K., Hao, C., Niki, H., Hastie, D. R., Taylor, R., and Roussel, P. B.: Measurements of alkyl and multifunctional organic nitrates at a rural site in Ontario, J. Geophys. Res., 100, 22795–22804, 1995.

O'Brien, J. M., Czuba, E., Hastie, D., Francisco, J. S., and Shepson, P. B.: Determination of the hydroxy nitrate yields from the reaction of C_2–C_6 alkenes with OH in the presence of NO, J. Phys. Chem. A, 102, 8903–8908, 1998.

Orlando, J. J., Tyndall, G. S., and Wallington, T. J.: The atmospheric chemistry of alkoxy radicals, Chem. Rev., 103, 4657–4689, 2003.

Ortega, J., Helmig, D., Guenther, A., Harley, P., Pressley, S., and Vogel, C.: Flux estimates and OH reaction potential of reactive biogenic volatile organic compounds (BVOCs) from a mixed northern hardwood forest, Atmos. Environ., 41, 5479–5495, 2007.

Ortega, J., Helmig, D., Daly, R. W., Tanner, D. M., Guenther, A. B., and Herrick, J. D.: Approaches for quantifying reactive and low-volatility biogenic organic compound emissions by vegetation enclosure techniques – Part B: Applications, Chemosphere, 72, 365–380, 2008.

Patchen, A. K., Pennino, M. J., Kiep, A. C., and Elrod, M. J.: Direct kinetics study of the product-forming channels of the reaction of isoprene-derived hydroxyperoxy radicals with NO, Int. J. Chem. Kinet., 39, 353–361, 2007.

Paulot, F., Crounse, J. D., Kjaergaard, H. G., Kroll, J. H., Seinfeld, J. H., and Wennberg, P. O.: Isoprene photooxidation: new insights into the production of acids and organic nitrates, Atmos. Chem. Phys., 9, 1479–1501, doi:10.5194/acp-9-1479-2009, 2009.

Peñuelas, J. and Staudt, M.: BVOCs and global change, Trends Plant Sci., 15, 133–144, 2010.

Perring, A. E., Bertram, T. H., Wooldridge, P. J., Fried, A., Heikes, B. G., Dibb, J., Crounse, J. D., Wennberg, P. O., Blake, N. J., Blake, D. R., Brune, W. H., Singh, H. B., and Cohen, R. C.: Airborne observations of total $RONO_2$: new constraints on the yield and lifetime of isoprene nitrates, Atmos. Chem. Phys., 9, 1451–1463, doi:10.5194/acp-9-1451-2009, 2009a.

Perring, A. E., Wisthaler, A., Graus, M., Wooldridge, P. J., Lockwood, A. L., Mielke, L. H., Shepson, P. B., Hansel, A., and Cohen, R. C.: A product study of the isoprene + NO_3 reaction, Atmos. Chem. Phys., 9, 4945–4956, doi:10.5194/acp-9-4945-2009, 2009b.

Pfrang, C., King, M. D., Canosa-Mas, C. E., and Wayne, R. P.: Structure-activity relations (SARs) for gas-phase reactions of NO_3, OH and O_3 with alkenes: an update, Atmos. Environ., 40, 1180–1186, 2006.

Pinto, D. M., Tiiva, P., Miettinen, P., Joutsensaari, J., Kokkola, H., Nerg, A.-M., Laaksonen, A., and Holopainen, J. K.: The effects of increasing atmospheric ozone on biogenic monoterpene profiles and the formation of secondary aerosols, Atmos. Environ., 41, 4877–4887, 2007.

Pollmann, J., Ortega, J., and Helmig, D.: Analysis of atmospheric sesquiterpenes: sampling losses and mitigation of ozone interferences, Environ. Sci. Technol., 39, 9620–9629, 2005.

Pressley, S., Lamb, B., Westberg, H., Flaherty, J., Chen, J., and Vogel, C.: Long-term isoprene flux measurements above a northern hardwood forest, J. Geophys. Res., 110, D07301, doi:10.1029/2004JD005523, 2005.

Raupach, M. R.: A practical Lagrangian method for relating scalar concentrations to source distributions in vegetation canopies, Q. J. Roy. Meteor. Soc., 115, 609–632, 1989.

Reissell, A., Arey, J., and Atkinson, R.: Atmospheric chemistry of camphor, Int. J. Chem. Kinet., 33, 56–63, 2001.

Ridley, B. A. and Grahek, F. E.: A small, low flow, high sensitivity reaction vessel for NO chemiluminescence detectors, J. Atmos. Ocean. Tech., 7, 307–311, 1990.

Rollins, A. W., Kiendler-Scharr, A., Fry, J. L., Brauers, T., Brown, S. S., Dorn, H.-P., Dubé, W. P., Fuchs, H., Mensah, A., Mentel, T. F., Rohrer, F., Tillmann, R., Wegener, R., Wooldridge, P. J., and Cohen, R. C.: Isoprene oxidation by nitrate radical: alkyl nitrate and secondary organic aerosol yields, Atmos. Chem. Phys., 9, 6685–6703, doi:10.5194/acp-9-6685-2009, 2009.

Rollins, A. W., Smith, J. D., Wilson, K. R., and Cohen, R. C.: Real time in situ detection of organic nitrates in atmospheric aerosols, Environ. Sci. Technol., 44, 5540–5545, 2010.

Ruppert, L. and Becker, K. H.: A product study of the OH radical-initiated oxidation of isoprene: formation of C_5-unsaturated diols, Atmos. Environ., 34, 1529–1542, 2000.

Salmond, J. A. and McKendry, I. G.: A review of turbulence in the very stable nocturnal boundary layer and its implications for air quality, Prog. Phys. Geog., 29, 171–188, 2005.

Schmid, H. P., Su, H.-B., Vogel, C. S., and Curtis, P. S.: Ecosystem-atmosphere exchange of carbon dioxide over a mixed hardwood forest in Northern Lower Michigan, J. Geophys. Res., 108, 4417, doi:10.1029/2002JD003011, 2003.

Shepson, P. B.: Organic nitrates, in: Volatile Organic Compounds in the Atmosphere, edited by: Koppmann, R., Blackwell Publishing Ltd., Ames, IA, 2007.

Sillman, S., Carroll, M. A., Thornberry, T., Lamb, B. K., Westberg, H., Brune, W. H., Faloona, I., Tan, D., Shepson, P. B., Sumner, A. L., Hastie, D. R., Mihele, C. M., Apel, E. C., Riemer, D. D., and Zika, R. G.: Loss of isoprene and sources of nighttime OH radicals at a rural site in the US: results from photochemical models, J. Geophys. Res., 107, 4043, doi:10.1029/2001JD000449, 2002.

Spanke, J., Rannik, Ü., Forkel, R., Nigge, W., and Hoffmann, T.: Emission fluxes and atmospheric degradation of monoterpenes above a boreal forest: field measurements and modelling, Tellus, 53B, 406–422, 2001.

Spittler, M., Barnes, I., Bejan, I., Brockmann, K. J., Benter, T., and Wirtz, K.: Reactions of NO_3 radicals with limonene and α-pinene: product and SOA formation, Atmos. Environ., 40, S116–S127, 2006.

Sprengnether, M., Demerjian, K. L., Donahue, N. M., and Anderson, J. G.: Product analysis of the OH oxidation of isoprene and 1,3-butadiene in the presence of NO, J. Geophys. Res., 107, 4268, doi:10.1029/2001JD000716, 2002.

Stroud, C., Makar, P., Karl, T., Guenther, A., Geron, C., Turnipseed, A., Nemitz, E., Baker, B., Potosnak, M., and Fuentes, J. D.: Role of canopy-scale photochemistry in modifying biogenic-atmosphere exchange of reactive terpene species: Results from the CELTIC field study, J. Geophys. Res., 110, D17303, doi:10.1029/2005JD005775, 2005.

Tan, D., Faloona, I., Simpas, J. B., Brune, W., Shepson, P. B., Couch, T. L., Sumner, A. L., Carroll, M. A., Thornberry, T., Apel, E., Riemer, D., and Stockwell, W.: HO_x budgets in a deciduous forest: results from the PROPHET summer 1998 campaign, J. Geophys. Res., 106, 24407–24427, 2001.

Thornberry, T., Carroll, M. A., Keeler, G. J., Sillman, S., Bertman, S. B., Pippin, M. R., Ostling, K., Grossenbacher, J. W., Shepson, P. B., Cooper, O. R., Moody, J. L., and Stockwell, W. R.: Observations of reactive oxidized nitrogen and speciation of NO_y during the PROPHET summer 1998 intensive, J. Geophys. Res., 106, 24359–24386, 2001.

Trainer, M., Buhr, M. P., Curran, C. M., Fehsenfeld, F. C., Hsie, E. Y., Liu, S. C., Norton, R. B., Parrish, D. D., Williams, E. J., Gandrud, B. W., Ridley, B. A., Shetter, J. D., Allwine, E. J., and Westberg, H. H.: Observations and modeling of the reactive nitrogen photochemistry at a rural site, J. Geophys. Res., 96, 3045–3063, 1991.

Tuazon, E. C. and Atkinson, R.: A product study of the gas-phase reaction of isoprene with the OH radical in the presence of NO_x, Int. J. Chem. Kinet., 22, 1221–1236, 1990.

USEPA: Estimation Programs Interface Suite™ for Microsoft® Windows, v 4.0, United States Environmental Protection Agency, Washington, DC, USA, 2010.

Wells, J. R.: Gas-phase chemistry of α-terpineol with ozone and OH radical: rate constants and products, Environ. Sci. Technol., 39, 6937–6943, 2005.

Werner, G., Kastler, J., Looser, R., and Ballschmiter, K.: Organic nitrates of isoprene as atmospheric trace compounds, Angew. Chem., 38, 1634–1637, 1999.

Wolfe, G. M. and Thornton, J. A.: The Chemistry of Atmosphere-Forest Exchange (CAFE) Model – Part 1: Model description and characterization, Atmos. Chem. Phys., 11, 77–101, doi:10.5194/acp-11-77-2011, 2011.

Wolfe, G. M., Thornton, J. A., Bouvier-Brown, N. C., Goldstein, A. H., Park, J.-H., McKay, M., Matross, D. M., Mao, J., Brune, W. H., LaFranchi, B. W., Browne, E. C., Min, K.-E., Wooldridge, P. J., Cohen, R. C., Crounse, J. D., Faloona, I. C., Gilman, J. B., Kuster, W. C., de Gouw, J. A., Huisman, A., and Keutsch, F. N.: The Chemistry of Atmosphere-Forest Exchange (CAFE) Model – Part 2: Application to BEARPEX-2007 observations, Atmos. Chem. Phys., 11, 1269–1294, doi:10.5194/acp-11-1269-2011, 2011a.

Wolfe, G. M., Thornton, J. A., McKay, M., and Goldstein, A. H.: Forest-atmosphere exchange of ozone: sensitivity to very reactive biogenic VOC emissions and implications for in-canopy photochemistry, Atmos. Chem. Phys., 11, 7875–7891, doi:10.5194/acp-11-7875-2011, 2011b.

Wu, S., Mickley, L. J., Jacob, D. J., Logan, J. A., Yantosca, R. M., and Rind, D.: Why are there large differences between models in global budgets of tropospheric ozone?, J. Geophys. Res., 112, D05302, doi:10.1029/2006JD007801, 2007.

Zhang, L., Brook, J. R., and Vet, R.: A revised parameterization for gaseous dry deposition in air-quality models, Atmos. Chem. Phys., 3, 2067–2082, doi:10.5194/acp-3-2067-2003, 2003.

Table 1. BVOCs identified during branch-enclosure emission measurements for UMBS tree species. Corresponding reaction rate constants for OH, O_3, and NO_3 at 298 K (k_{OH}, k_{O_3}, and k_{NO_3}, respectively) and $RONO_2$ yields for reactions with OH and NO_3 (γ_{OH} and γ_{NO_3}, respectively) are included for each BVOC identified.

BVOC	Structure	k_{OH} k_{O3} k_{NO3} (cm^3 $molec^{-1}$ s^{-1})	$RONO_2$: γ_{OH} γ_{NO3}
Isoprene (C_5H_8)	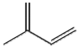	1.0 x 10^{-10} a) 1.27 x 10^{-17} a) 7.0 x 10^{-13} a)	0.07 b) 0.68 c)
norbornene (C_7H_{10})		1.0 x 10^{-10} d) 1.27 x 10^{-17} d) 7.0 x 10^{-13} d)	0.11 e) 0.31 f)
p-cymene ($C_{10}H_{14}$)	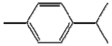	1.51 x 10^{-11} g) (<)5 x 10^{-20} h) 9.9 x 10^{-16} g)	0.03 i) 0.31 f)
o-cymene ($C_{10}H_{14}$)	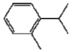	8.54 x 10^{-12} j) (<)5 x 10^{-20} k) 9.9 x 10^{-16} k)	0.03 i) 0.31 f)
cyclofenchone ($C_{10}H_{16}$)		3.54 x 10^{-12} j) (<)1 x 10^{-23} d) 1.4 x 10^{-15} l)	0.31 m) 0.31 f)
tricyclene ($C_{10}H_{16}$)		2.66 x 10^{-12} j) (<)1 x 10^{-23} d) 1.1 x 10^{-15} l)	0.31 m) 0.31 f)
α-pinene ($C_{10}H_{16}$)	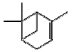	5.3 x 10^{-11} a) 9.0 x 10^{-17} a) 6.16 x 10^{-12} d)	0.18 n) 0.20 o)
α-thujene ($C_{10}H_{16}$)	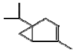	7.10 x 10^{-11} p) 6.2 x 10^{-17} p) 5.5 x 10^{-12} q)	0.18 e) 0.31 f)
4-carene ($C_{10}H_{16}$)	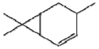	5.81 x 10^{-11} j) 2.00 x 10^{-16} j) 8.9 x 10^{-13} q)	0.18 e) 0.31 f)
β-pinene ($C_{10}H_{16}$)	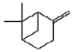	7.43 x 10^{-11} d) 1.5 x 10^{-17} d) 2.51 x 10^{-12} d)	0.23 r) 0.43 s)
camphene ($C_{10}H_{16}$)		5.30 x 10^{-11} d) 9.0 x 10^{-19} d) 6.6 x 10^{-13} d)	0.23 t) 0.31 f)
sabinene ($C_{10}H_{16}$)	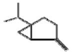	1.17 x 10^{-10} d) 8.3 x 10^{-17} d) 1.0 x 10^{-11} d)	0.23 t) 0.31 f)
α-terpinene ($C_{10}H_{16}$)	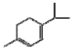	3.63 x 10^{-10} d) 2.1 x 10^{-14} d) 1.4 x 10^{-11} d)	0.18 e) 0.31 f)
γ-terpinene ($C_{10}H_{16}$)	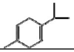	1.77 x 10^{-10} d) 1.4 x 10^{-16} d) 2.9 x 10^{-11} d)	0.18 e) 0.31 f)

Table 1. Continued.

α-phellandrene $(C_{10}H_{16})$	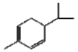	3.13 x 10^{-10} d) 3.0 x 10^{-15} d) 7.3 x 10^{-11} d)	0.18 e) 0.31 f)
β-phellandrene $(C_{10}H_{16})$	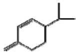	1.68 x 10^{-10} d) 4.7 x 10^{-17} d) 8.0 x 10^{-12} d)	0.18 e) 0.31 f)
terpinolene $(C_{10}H_{16})$	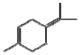	2.25 x 10^{-10} d) 1.9 x 10^{-15} d) 9.7 x 10^{-11} d)	0.18 e) 0.31 f)
limonene $(C_{10}H_{16})$	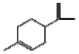	1.64 x 10^{-10} d) 2.1 x 10^{-16} d) 1.22 x 10^{-11} d)	0.28 u) 0.30 ee)
β-myrcene $(C_{10}H_{16})$	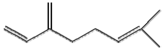	3.35 x 10^{-10} v) 3.85 x 10^{-16} v) 1.1 x 10^{-11} d)	0.18 e) 0.31 f)
allo-ocimene $(C_{10}H_{16})$		2.36 x 10^{-10} j) 4.16 x 10^{-16} j) 1.1 x 10^{-11} q)	0.18 e) 0.31 f)
cis-ocimene $(C_{10}H_{16})$	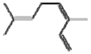	3.03 x 10^{-10} v) 3.85 x 10^{-16} v) 2.20 x 10^{-11} d)	0.18 e) 0.31 f)
trans-ocimene $(C_{10}H_{16})$		3.03 x 10^{-10} v) 3.85 x 10^{-16} v) 2.20 x 10^{-11} d)	0.18 e) 0.31 f)
3-carene $(C_{10}H_{16})$	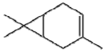	8.80 x 10^{-11} d) 3.7 x 10^{-17} d) 9.1 x 10^{-12} d)	0.18 e) 0.31 f)
para-cymenene $(C_{10}H_{16})$	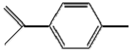	5.7 x 10^{-11} j) 1.4 x 10^{-16} j) 1.5 x 10^{-12} ff)	0.18 e) 0.31 f)
dimethylnonatriene $(C_{11}H_{18})$	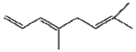	2.32 x 10^{-10} j) 7.50 x 10^{-16} j) 9.6 x 10^{-12} q)	0.20 e) 0.31 f)
camphor $(C_{10}H_{16}O)$		4.30 x 10^{-12} d) (<)7 x 10^{-20} w) (<)3.00 x 10^{-16} d)	0.31 m) 0.31 f)
1,8-cineole $(C_{10}H_{18}O)$		1.11 x 10^{-11} g) (<)1.5 x 10^{-19} h) 1.7 x 10^{-16} g)	0.52 x) 0.31 f)
camphene hydrate $(C_{10}H_{18}O)$	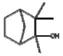	9.43 x 10^{-12} j) (<)1 x 10^{-20} d) 6.4 x 10^{-16} l)	0.52 x) 0.31 f)
borneol $(C_{10}H_{18}O)$	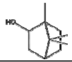	1.14 x 10^{-11} j) (<)1 x 10^{-20} d) 4.6 x 10^{-15} l)	0.52 x) 0.31 f)

Table 1. Continued.

4-terpineol $(C_{10}H_{18}O)$	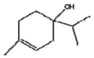	1.04 x 10^{-10} j) (<)1 x 10^{-20} j) 1.4 x 10^{-16} q)	0.30 y) 0.31 f)
α-terpineol $(C_{10}H_{18}O)$	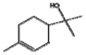	1.9 x 10^{-10} z) 3.0 x 10^{-16} z) 1.60 x 10^{-11} aa)	0.30 y) 0.31 f)
β-linalool $(C_{10}H_{18}O)$	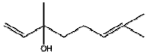	1.59 x 10^{-10} bb) 4.3 x 10^{-16} bb) 1.12 x 10^{-11} bb)	0.30 y) 0.31 f)
cis- and *trans*- linalool oxide $(C_{10}H_{18}O_2)$	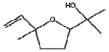	6.68 x 10^{-11} j) 1.75 x 10^{-18} j) 4.6 x 10^{-14} q)	0.30 y) 0.31 f)
α-copaene $(C_{15}H_{24})$	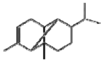	9.00 x 10^{-11} d) 1.60 x 10^{-16} d) 1.60 x 10^{-11} d)	0.29 e) 0.31 f)
α-cubebene $(C_{15}H_{24})$	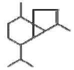	1.00 x 10^{-10} j) 4.30 x 10^{-16} d) 7.9 x 10^{-12} q)	0.29 e) 0.31 f)
α-cedrene $(C_{15}H_{24})$		6.70 x 10^{-11} d) 2.80 x 10^{-17} d) 8.20 x 10^{-12} d)	0.29 e) 0.31 f)
β-bourbonene $(C_{15}H_{24})$	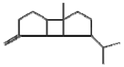	6.19 x 10^{-11} j) 1.2 x 10^{-17} j) 3.5 x 10^{-13} q)	0.29 e) 0.31 f)
β-cubebene $(C_{15}H_{24})$	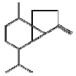	6.54 x 10^{-11} j) 1.20 x 10^{-17} j) 3.5 x 10^{-13} q)	0.29 e) 0.31 f)
β-gurjunene $(C_{15}H_{24})$	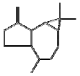	6.01 x 10^{-11} j) 1.20 x 10^{-17} j) 3.5 x 10^{-13} q)	0.29 e) 0.31 f)
aromadendrene $(C_{15}H_{24})$	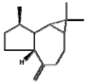	1.50 x 10^{-10} cc) 6.50 x 10^{-15} dd) 3.5 x 10^{-13} q)	0.29 e) 0.31 f)
allo- aromadendrene $(C_{15}H_{24})$	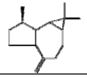	6.25 x 10^{-11} j) 1.20 x 10^{-17} j) 3.5 x 10^{-13} q)	0.29 e) 0.31 f)

Title Page
Abstract Introduction
Conclusions References
Tables Figures
◄◄ ►►
◄ ►
Back Close
Full Screen / Esc
Printer-friendly Version
Interactive Discussion

Table 1. Continued.

β-caryophyllene ($C_{15}H_{24}$)	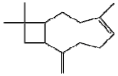	1.97×10^{-11} d) 1.16×10^{-14} d) 1.9×10^{-11} d)	0.29 e) 0.31 f)
γ-cadinene ($C_{15}H_{24}$)	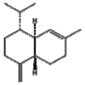	1.56×10^{-10} j) 3.20×10^{-14} dd) 5.9×10^{-12} q)	0.29 e) 0.31 f)
γ-muurolene ($C_{15}H_{24}$)	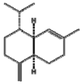	1.56×10^{-10} j) 4.42×10^{-16} j) 5.9×10^{-12} q)	0.29 e) 0.31 f)
α-selinene ($C_{15}H_{24}$)	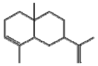	1.51×10^{-10} j) 4.42×10^{-16} j) 5.8×10^{-12} q)	0.29 e) 0.31 f)
α-*trans*-bergamotene ($C_{15}H_{24}$)	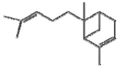	1.80×10^{-10} j) 8.60×10^{-16} j) 9.6×10^{-12} q)	0.29 e) 0.31 f)
β-selinene ($C_{15}H_{24}$)	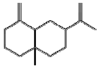	1.17×10^{-10} j) 2.40×10^{-17} j) 6.5×10^{-13} q)	0.29 e) 0.31 f)
δ-cadinene ($C_{15}H_{24}$)	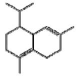	2.11×10^{-10} j) 1.63×10^{-15} j) 5.2×10^{-11} q)	0.29 e) 0.31 f)
α-muurolene ($C_{15}H_{24}$)	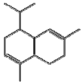	1.90×10^{-10} j) 8.6×10^{-16} j) 1.1×10^{-11} q)	0.29 e) 0.31 f)
β-elemene ($C_{15}H_{24}$)	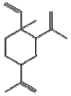	1.40×10^{-10} j) 2.6×10^{-17} j) 6.3×10^{-11} q)	0.29 e) 0.31 f)
germacrene B ($C_{15}H_{24}$)	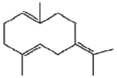	2.90×10^{-10} j) 2.06×10^{-15} j) 4.3×10^{-11} q)	0.29 e) 0.31 f)
D germacrene ($C_{15}H_{24}$)	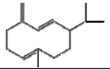	2.40×10^{-10} j) 6.10×10^{-16} j) 6.4×10^{-12} q)	0.29 e) 0.31 f)

Table 1. Continued.

α-humulene ($C_{15}H_{24}$)	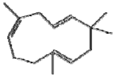	2.93×10^{-10} d) 1.17×10^{-14} d) 3.90×10^{-11} d)	0.29 e) 0.31 f)
β-farnesene ($C_{15}H_{24}$)	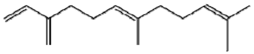	2.88×10^{-10} v) 6.86×10^{-16} v) 9.3×10^{-12} q)	0.29 e) 0.31 f)
α-farnesene ($C_{15}H_{24}$)	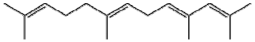	2.19×10^{-10} v) 5.94×10^{-16} v) 2.1×10^{-11} q)	0.29 e) 0.31 f)
β-bisabolene ($C_{15}H_{24}$)	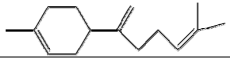	2.4×10^{-11} j) 8.7×10^{-16} j) 9.2×10^{-12} q)	0.29 e) 0.31 f)

a) Atkinson et al. (2006); b) Lockwood et al. (2010); c) Average of Perring et al. (2009b) and Rollins et al. (2009); d) Atkinson and Arey (2003a); e) Estimated based on Arey et al. (2001) and O'Brien et al. (1998); f) Average of α-pinene, β-pinene, and limonene yields; g) Corchnoy and Atkinson (1990); h) Atkinson et al. (1990); i) p-xylene (Espada et al., 2005) used as a proxy; j) Estimated using the Environmental Protection Agency's Estimation Program Interface Suite (USEPA, 2010); k) p-cymene used as a proxy; l) Estimated based on Kerdouci et al. (2010); m) Estimated based on Arey et al. (2001); n) Nozière et al. (1999); o) Spittler et al. (2006); p) Pinto et al. (2007); q) Estimated based on Pfrang et al. (2006); r) Davis et al. (2005); s) Fry et al. (2009); t) β-pinene used as a proxy; u) Leungsakul et al. (2005); v) Kim et al. (2011a); w) Reissell et al. (2001); x) Estimated based on Arey et al. (2001) and Espada and Shepson (2005); y) Estimated based on Arey et al. (2001), Espada and Shepson (2005), and O'Brien et al. (1998); z) Wells (2005); aa) Jones and Ham (2008); bb) Atkinson et al. (1995); cc) Ng et al. (2007); dd) Pollmann et al. (2005); ee) Fry et al. (2011); ff) styrene (Atkinson and Arey, 2003a) used as a proxy.

Table 2. Individual primary isoprene nitrate relative yields and corresponding rate constants (units of $cm^3 molec^{-1} s^{-1}$) are shown; secondary isoprene nitrate yields for reaction with OH are shown with the specific species listed in parentheses and shown in Table 3. All primary isoprene nitrates are assumed to have secondary $RONO_2$ yields of 0.50 for reaction with O_3. For reaction of all primary isoprene nitrates with NO_3, yields are assumed to be 0.60 (containing one nitrate group) and 0.40 (dinitrate yield) based on Rollins et al. (2009).

Isoprene Nitrate	Structure	Relative $RONO_2$ γ_{OH} γ_{NO3}	k_{OH} k_{O3} k_{NO3}	Secondary $RONO_2$ (γ_{OH})
$RONO_2$-4,3	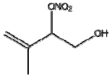	0.63 a) 0 b)	5.3×10^{-11} c) 3.7×10^{-17} d) 3.0×10^{-13} d)	0.40 (MVKN) e)
$RONO_2$-3,4	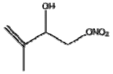	0.013 a) 0 b)	5.3×10^{-11} c) 3.7×10^{-17} d) 3.0×10^{-13} d)	0.15 (MVKN) e); 0.30 (ETHLN) e)
$RONO_2$-1,2	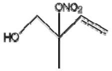	0.183 a) 0 b)	1.4×10^{-11} c) 1.4×10^{-17} d) 4.6×10^{-14} d)	0.40 (MACRN) e)
$RONO_2$-2,1	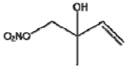	0.0747 a) 0 b)	2.8×10^{-11} c) 1.4×10^{-17} d) 4.6×10^{-14} d)	1.0 (PROPNN) e)
$RONO_2$-4,1		0.0795 a) 0.2 b)	4.5×10^{-11} c) 1.6×10^{-16} d) 4.8×10^{-12} d)	0.30 (PROPNN) e)
$RONO_2$-1,4	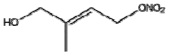	0.0195 a) 0 b)	4.5×10^{-11} c) 1.6×10^{-16} d) 4.8×10^{-12} d)	0.15 (MVKN) e); 0.30 (ETHLN) e)
NO_3-NITROX	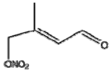	0 a) 0.8 b)	3.1×10^{-11} c) 3×10^{-18} b) 5.5×10^{-12} d)	0.30 (PROPNN) b)

a) Costa (2011) (Correction to Lockwood et al. (2010) yields); b) Rollins et al. (2009); c) Estimated using the Environmental Protection Agency's Estimation Program Interface Suite (USEPA, 2010); d) Estimated based on Pfrang et al. (2006); e) Paulot et al. (2009).

Table 3. Secondary isoprene nitrates and corresponding rate constants (units of $cm^3 molec^{-1} s^{-1}$).

Isoprene Nitrate	Structure	k_{OH} k_{O3} k_{NO3}
MACRN	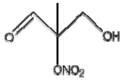	5.0×10^{-11} a) (<)1×10^{-20} b) 9.6×10^{-16} c)
MVKN	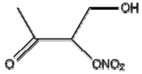	5.6×10^{-12} a) (<)1×10^{-20} b) 4.7×10^{-15} c)
ETHLN		1.0×10^{-11} a) (<)1×10^{-20} b) 2.9×10^{-16} c)
PROPNN	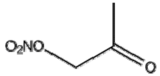	4.9×10^{-13} a) (<)1×10^{-20} b) 9.4×10^{-16} c)

a) Paulot et al. (2009);
b) Atkinson et al. (1990);
c) Estimated based on Kerdouci et al. (2010).

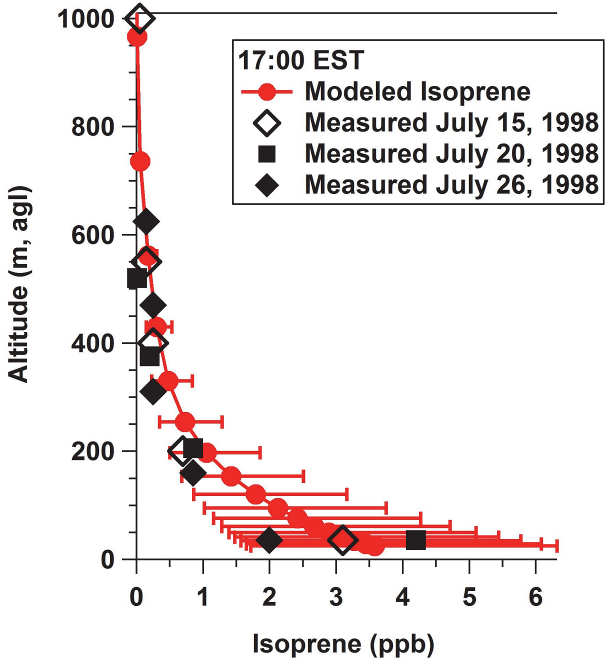

Fig. 1. Comparison of modeled and measured (Hurst et al., 2001) vertical profiles of isoprene concentrations at UMBS. Error bars represent sensitivity to the range of isoprene emission rates.

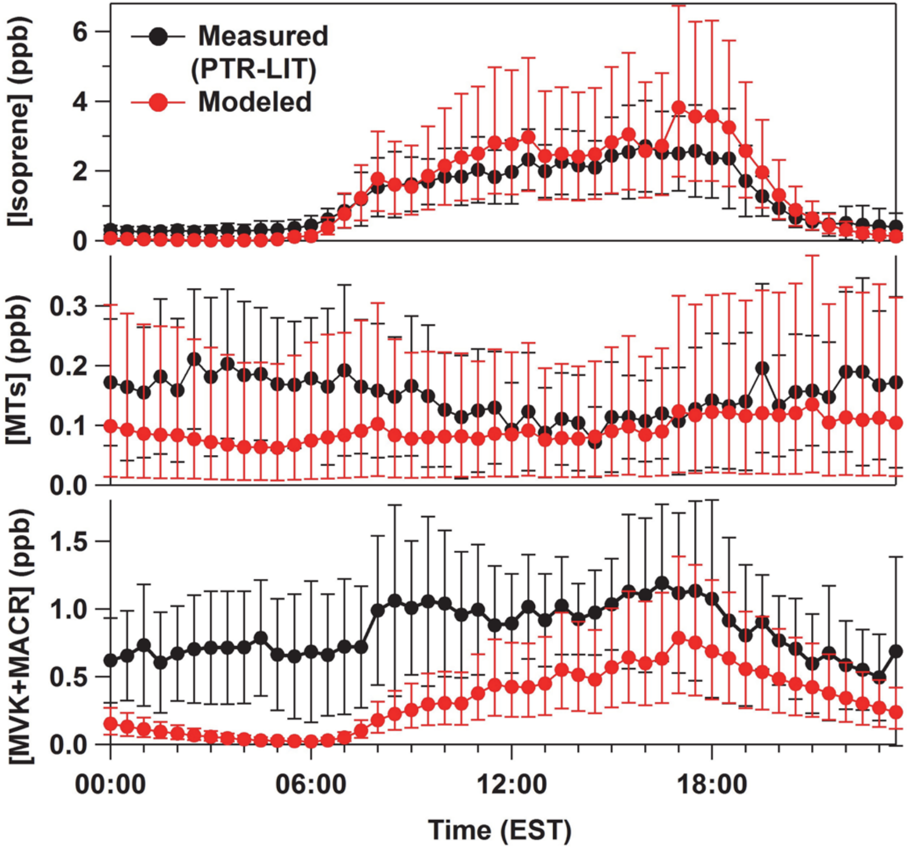

Fig. 2. Diurnal cycles of modeled and measured [isoprene], [total monoterpenes (MTs)], and [methyl vinyl ketone (MVK) + methacrolein (MACR)] at ∼12 m above the forest canopy. July–August 2008 measurements were completed using a proton-transfer reaction linear ion trap mass spectrometer (PTR-LIT) (Mielke et al., 2010). Sensitivity to uncertainties and variability are indicated by error bars.

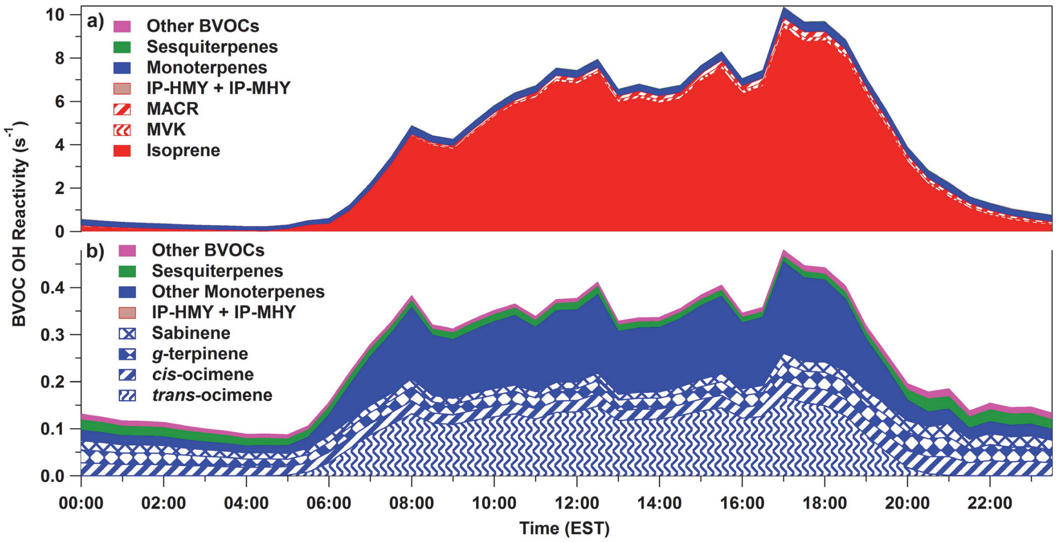

Fig. 3. OH reactivity at ~12 m above the forest canopy for average concentrations of **(a)** all BVOCs plus first generation isoprene oxidation products and **(b)** only compounds not considered by Di Carlo et al. (2004). OH reactivities are shown for the base BVOC production rate scenario. First generation isoprene oxidation products included are methyl vinyl ketone (MVK), methacrolein (MACR), and C_5-unsaturated hydroxyaldehyde isomers (IP-HMY and IP-MHY).

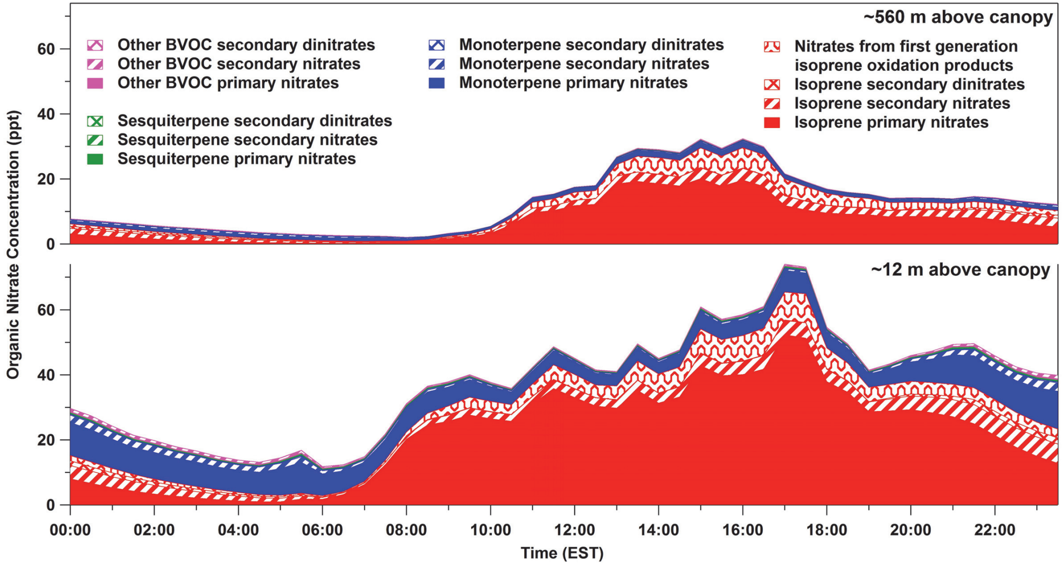

Fig. 4. Diurnal cycles of modeled organic nitrate concentrations at ~560 m and ~12 m above the forest canopy. At ~12 m above the forest canopy, sesquiterpene and other BVOC nitrates possessed similar temporal trends with a minimum total concentration of 0.6 ppt in the midday (12:30 EST) and a maximum of 2.1 ppt at 23:30 EST. In comparison, at ~560 m above the forest canopy, the total concentration of sesquiterpene and other BVOC nitrates ranged from 0.1–0.4 ppt through the course of the day. Results for the base BVOC production rate scenario are shown.

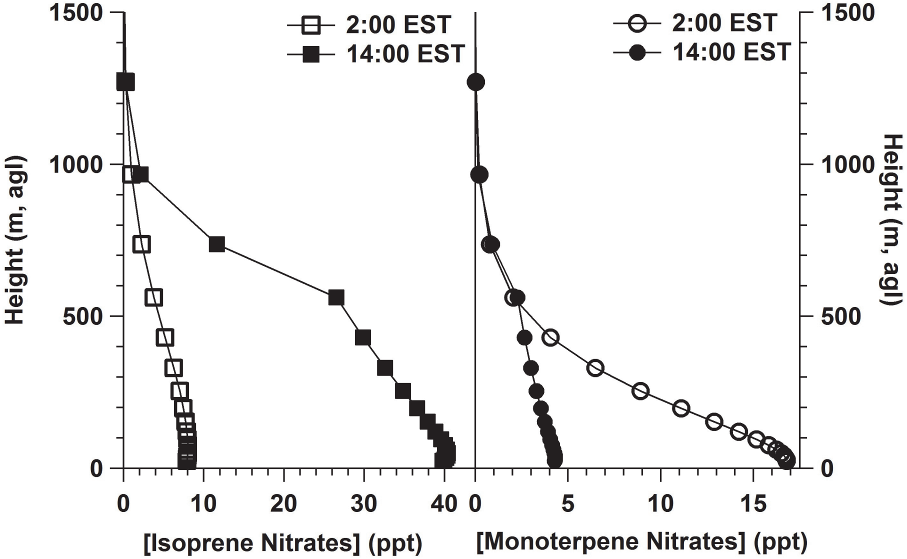

Fig. 5. Vertical profiles of total (primary and secondary) isoprene (left) and monoterpene (right) nitrate concentrations above the forest canopy at 02:00 and 14:00 EST for the base emission rate scenario. Total isoprene nitrates include nitrates formed from first generation isoprene oxidation products (methacrolein, methyl vinyl ketone, and C_5-unsaturated hydroxyaldehyde isomers).

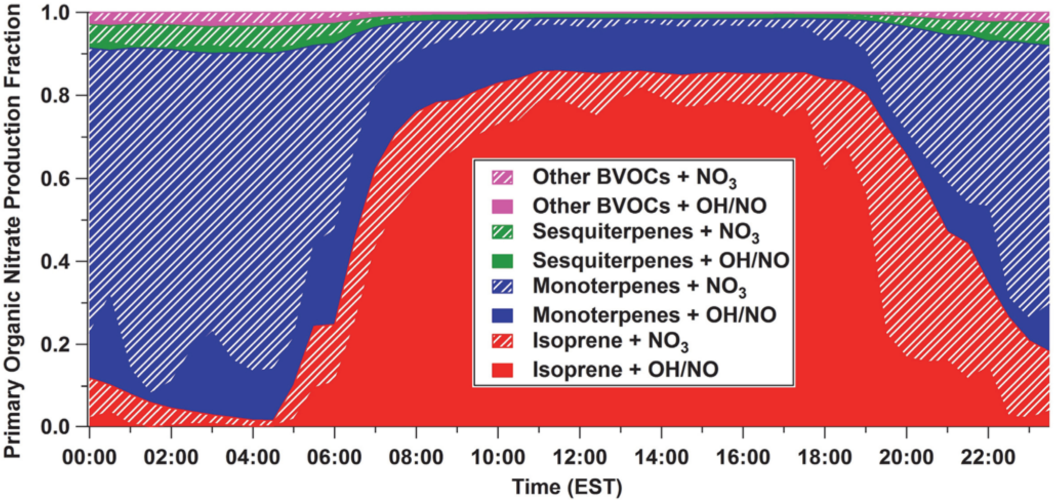

Fig. 6. Diurnal cycle of fractional modeled primary organic nitrate production at ∼12 m above the forest canopy. Results for the base BVOC production rate scenario are shown.

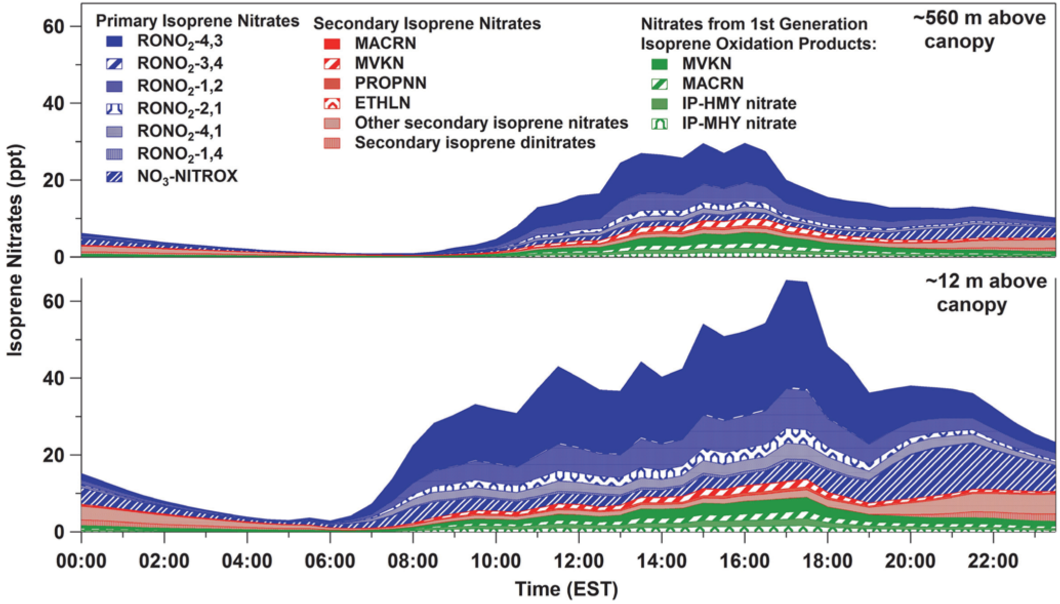

Fig. 7. Diurnal cycles of the modeled concentrations of isoprene nitrates at ~12 and ~560 m above the forest canopy for the base isoprene production rate scenario. Structures of specific primary and secondary isoprene nitrates are shown in Tables 2 and 3.

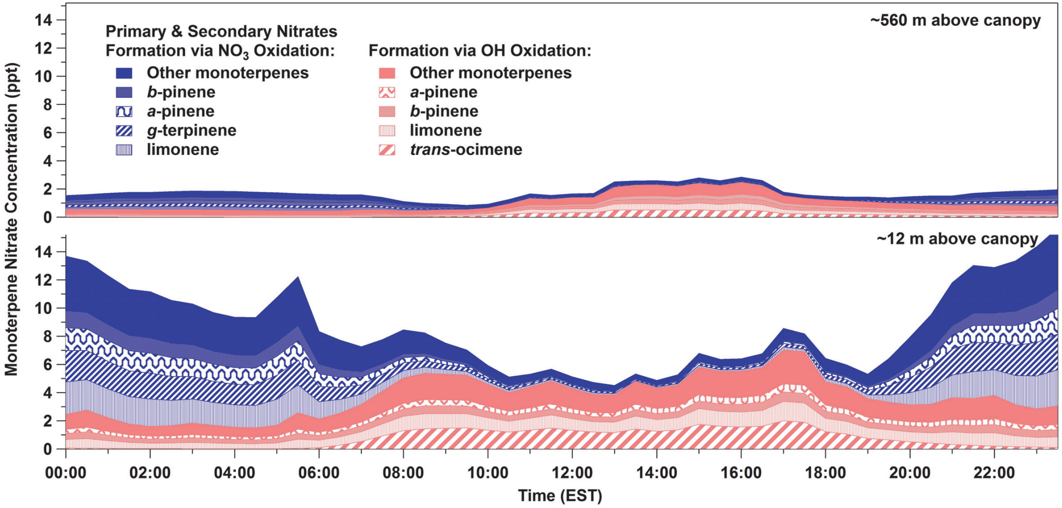

Fig. 8. Diurnal cycles of modeled monoterpene nitrate (including both primary and secondary species; oxidant refers to initial reaction) concentrations at ∼560 m and ∼12 m above the forest canopy. Results for the base BVOC production rate scenario are shown.